INSTITUTE OF ELECTRONIC MATERIALS TECHNOLOGY

MATERIAŁY ELEKTRONICZNE

ELECTRONIC MATERIALS

QUARTERLY

Vol. 45, No. 2 - 4
2017

Creating the English language version of the journal „Electronic Materials" and digitalization of „Electronic Materials" to provide and maintain open access through the Internet - tasks financed in accordance with the 593/P-DUN/2017 agreement from the funds of the Ministry of Science and Higher Education intendend for the science dissemination.

WARSAW ITME 2017

MATERIAŁY ELEKTRONICZNE
ELECTRONIC MATERIALS

Vol. 45 No. 2 - 4 2017

CONTENTS

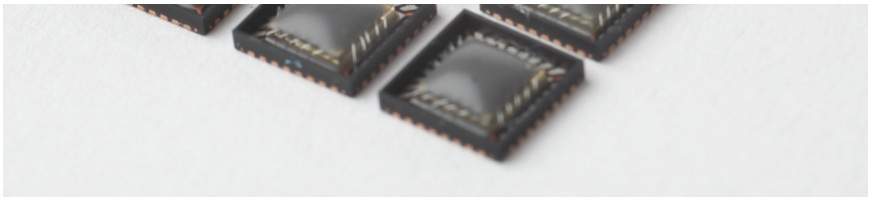

On the cover:
Graphene-based magnetic field sensors made in ITME.

Authors of the device: Tymoteusz Ciuk, Andrzej Kowalik, Iwona Jóźwik, Włodzimierz Strupiński

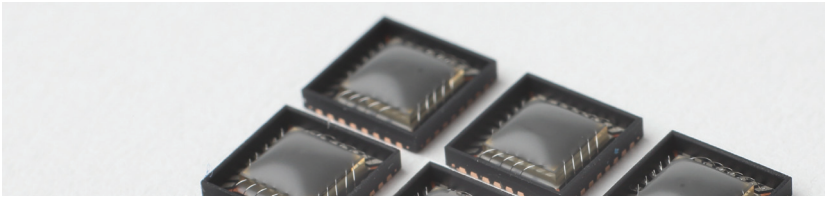

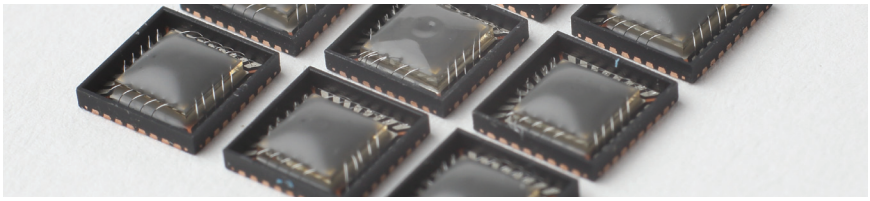

EDITORIAL OFFICE ADDRESS

Institute of Electronic Materials Technology
Wólczyńska Str. 133, 01-919 Warsaw
e-mail: ointe@itme.edu.pl
www: matelektron.itme.edu.pl

CONTACT

Editor in Chief phone: (22) 639 58 85
Editorial Assistant phone: (22) 639 55 29

PL ISSN 0209 - 0058

A quarterly quoted on the list of scientific journals of the Ministry of Science and Higher Education
7 points - according to the statement of the Ministry of Science and Higher Education.

Published articles are indexed in databases:
BazTech, CAS - Chemical Abstracts

Published articles of a scientific nature are reviewed by independent researchers.

The paper version is the primary version.

The quarterly is published in open access.

Circulation: 200 copies

Influence of gold electrodes on the properties of shear horizontal acoustic plate mode viscosity sensor in BT-cut quartz

Waldemar Soluch[1], Magdalena Łysakowska[1], Tadeusz Wróbel[1]

Until now the influence of gold electrodes on the properties of shear horizontal acoustic plate modes (SHAPMs) in BT-cut quartz (-50.5°YX90°) was never before calculated or measured. Calculation presented in this study show that the amplitude of mechanical motion at the quartz plate surface decreases with an increase of the thickness of the gold layer. When the thickness of the gold layer is increased only on one side of the quartz plate, the amplitude decreases on the same side, whereas it remaines unchanged on the opposite side. For one of the SHAPMs, the amplitude of mechanical motion become about twice as big when the gold layer thickness increased from about 0.1 μm to 1 μm. This effect was confirmed by the measurements of the changes of the delay line insertion loss against viscosity of glycerine and water solutions.

Key words: shear horizontal acoustic plate modes, BT-cut quartz, gold electrodes, delay line, insertion loss, viscosity sensor

Wpływ złotych elektrod na właściwości czujnika z poprzecznym horyzontalnym akustycznym modem płytowym w kwarcu o orientacji BT

Po raz pierwszy wykonano obliczenia i pomiary wpływu złotych elektrod na właściwości czujnika lepkości z poprzecznym horyzontalnym akustycznym modem płytowym (PHAMP) w kwarcu o orientacji BT (-50.5°YX90°). Stwierdzono, że amplituda drgań mechanicznych na powierzchni płytki kwarcowej maleje wraz ze wzrostem grubości warstwy złota. Gdy grubość warstwy złota wzrasta po jednej stronie płytki kwarcowej, to zmniejszanie ma miejsce po tej samej stronie, podczas gdy pozostaje niezmienione po stronie przeciwnej. Dla jednego z PHAMP, amplituda drgań mechanicznych zmalała dwa razy gdy grubość warstwy złota wzrosła od 0,1 μm do 1 μm. Efekt ten został potwierdzony przez pomiar zmian tłumienności linii opóźniającej w funkcji lepkości roztworów gliceryny i wody.

Słowa kluczowe: poprzeczne horyzontalne akustyczne mody płytowe, kwarc o orientacji BT, złote elektrody, linia opóźniająca, tłumienność wtrącenia, czujnik lepkości

1. Introduction

Shear horizontal acoustic plate modes (SHAPMs) in BT-cut quartz (-50.5°YX90°) are attractive for application in viscosity sensors [1]. However, previous calculations of the SHAPMs properties were done on the undestanding that the thickness of electrodes deposited on both sides of the BT-cut quartz plate is infinitesimally small. Because the finite thickness of the electrodes is used in practical applications, it is important that the influence of the thickness on the SHAPMs properties become calculated and measured. Compared to aluminium, gold is more convenient for the fabrication of larger thicknesses of layers and is much more resistant to mechanical and chemical undesirable effects in liquid sensors. This paper presents calculations and measurements results of the influence of finite thickness of gold electrodes on the properties of SHAPM viscosity sensor in BT-cut quartz.

2. Calculation method and results

Compared to the case of infinitesimally thin metal layers [1], new algorithm and computer program were developed to solve the problem of SHAPMs in the case of finite thickness of isotropic metal layers deposited on both sides of a piezoelectric plate (Fig. 1). Here, X, Y', Z' and x_1, x_2, x_3 are the crystallographic and wave coordinate systems, respectively. In this case, equations of motion were solved in the piezoelectric plate and in both isotropic metal layers of different thicknesses. By applying mechanical and electrical boundary conditions as used in the case of Love wave [2], properties of SHAPMs in BT-cut quartz were calculated for $h/\lambda = 14$, where h is the quartz plate thickness and λ is the acoustic wavelength [1].

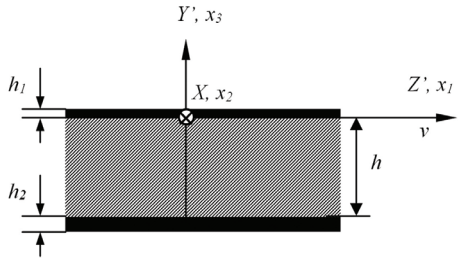

Fig. 1. BT-cut quartz plate with gold electrodes and coordinate systems.
Rys. 1. Płytka kwarcu o orientacji BT ze złotymi elektrodami i układy współrzędnych.

[1] *Institute of Electronic Materials Technology*, 133 Wólczyńska Str., 01-919 Warsaw, Poland e-mail: w.soluch@op.pl

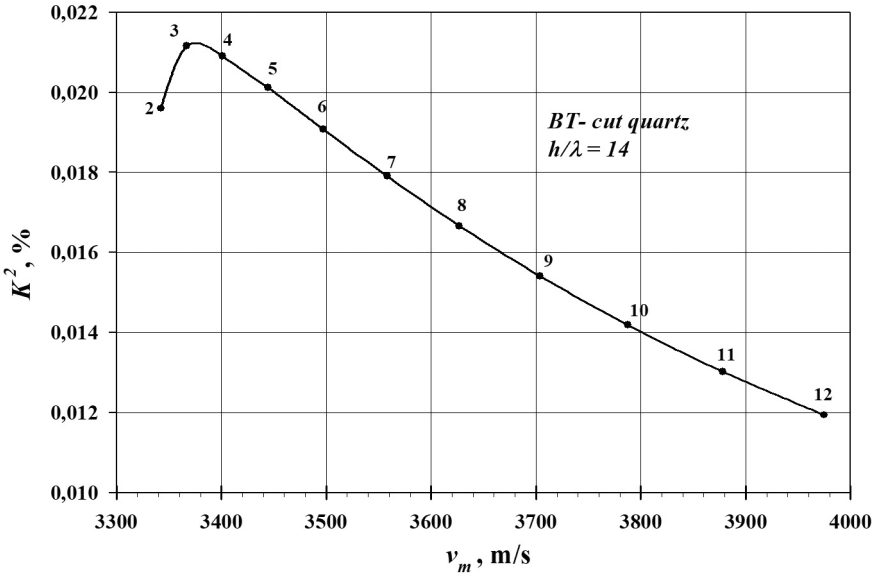

Fig. 2. Electromechanical coupling coefficient against SHAPMs velocity for $h_1 = h_2 = 0.1$ μm.
Rys. 2. Współczynnik sprzężenia elektromechaniczneg PHAMP w funkcji prędkości dla $h_1 = h_2 = 0{,}1$ μm.

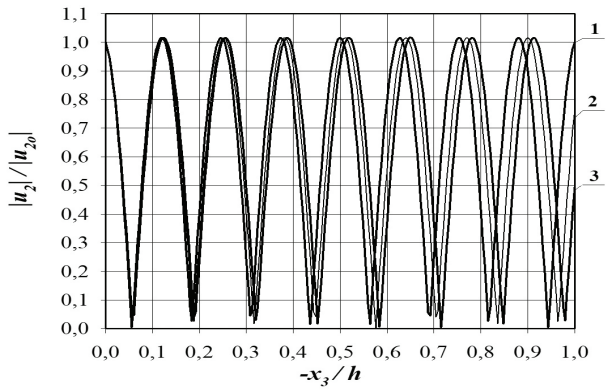

Fig. 3. Distributions of relative u_2 mechanical component amplitudes of the 8th mode for different values of h_2: 1- $h_2 = 0.1$ μm; 2- $h_2 = 0.5$ μm; 3- $h_2 = 1$ μm.
Rys. 3. Rozkłady względnych amplitud mechanicznych u_2 dla modu ósmego przy różnych wartościach h_2: 1- $h_2 = 0{,}1$ μm; 2- $h_2 = 0{,}5$ μm; 3- $h_2 = 1$ μm.

The results of calculations of the electromechanical coupling coefficient K^2 against velocity v_m of the metallised plate are shown in Fig. 2. Compared to the case with infinitesimally thin electrodes [1], there are significant differences of K^2 for the first several modes, whereas above this area, present calculations gave slightly higher values of K^2. It was also found that the effect of gold electrodes thickness on K^2 is very small and can be neglected.

As in the previous work [1], arbitrarily chosen 8th mode, located near the center of the spectrum, was used for the calculations. Calculated amplitude distributions of mechanical displacements of this mode is shown in Fig. 3. It can be seen that the amplitude of u_2 decreases only on the side of the plate at which the gold layer thickness h_2 was increased. It means that maximum sensitivity to viscosity changes will exist for thin gold layer.

3. Measurement methods and results

The same delay line as in [1] was used for the measurements (Fig. 4). A gold layer thickness of about 0.2 μm was used for the delay line, which is approximately equivalent to $h_1 = 0.1$ μm of continues layer used in the calculations [2]. The opposite plane was covered with a 0.1 μm thick continues gold layer. The delay line was mounted in a metal package, with a window for liquid loading. The measured amplitude spectrum and the 8th mode in air (Network Analyzer Type 8753ET, Agilent Technologies, Inc., Santa Clara, CA), with 60 nH parallel inductors [1], are shown in Fig. 5 and 6, respectively. It can be seen that the results are approximately the same as the one that were obtained for 0.6 μm thick aluminium electrodes deposited on the delay line side of the quartz plate[1]. Markers 1 and 2 indicate the surface transverse wave (STW) and the 8th mode, respectively.

Changes of insertion loss ΔIL against $\sqrt{\rho\eta}$, where ρ and η are the mass density and dynamic viscosity of glycerine and water solutions, respectively, were measured

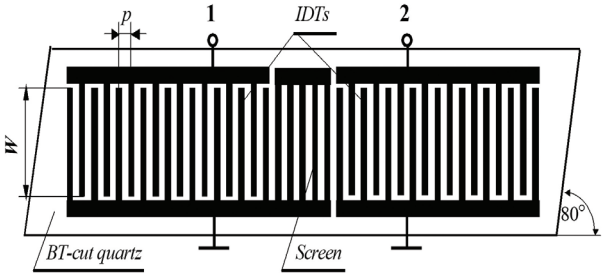

Fig. 4. Structure of the delay line.
Rys. 4. Struktura linii opóźniającej.

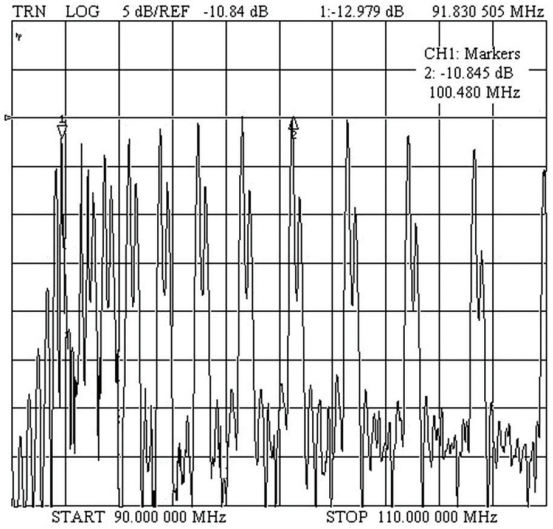

Fig. 5. Amplitude spectrum of SHAPMs in air for $h_1 = h_2 =$ 0.1 μm.
Rys. 5. Widmo amplitudowe PHAMP w powietrzu dla $h_1 = h_2 =$ 0,1 μm.

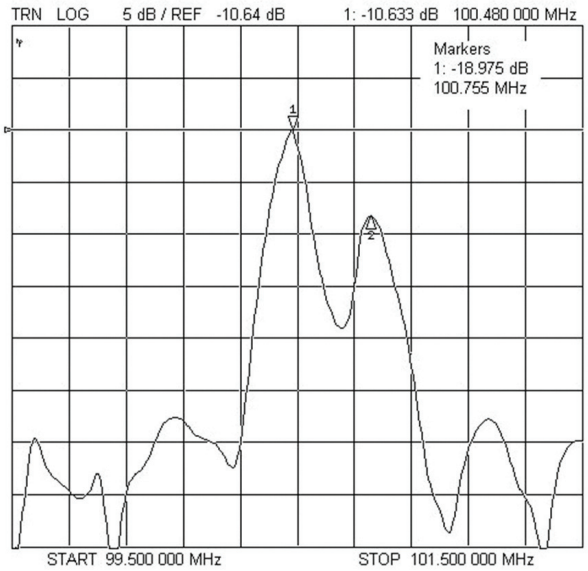

Fig. 6. Amplitude response of the 8th SHAPM.
Rys. 6. Charakterystyka amplitudowa ósmego modu PHMP.

at room temperature for different values of h_2 (Fig. 7). For $h_1 = h_2 = 0.1$ μm in a viscosity range from about 1 mPa·s to 1000 mPa·s, the insertion loss change was of about 14 dB. This value is approximately the same as the value obtained for aluminium electrodes [1]. It can be seen that the sensitivity to viscosity changes decrease with an increase of h_2.

4. Conclusions

It was found that for SHAPMs, amplitude of mechanical motion on the plate surface decreases with an increase of

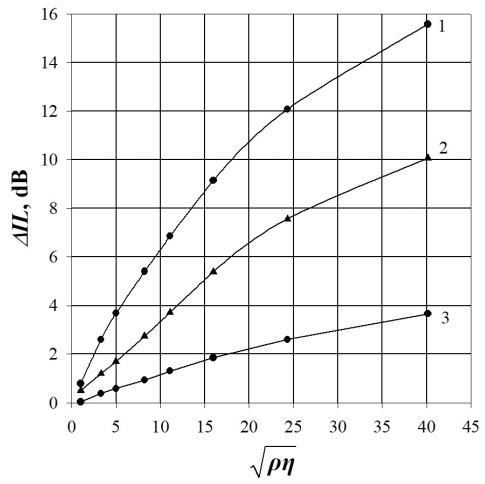

Fig. 7. Insertion loss changes for different thicknesses of gold layer (ρ [g/cm^3], η [mPa·s): 1- $h_2 = 0.1$ μm; 2- $h_2 = 0.5$ μm; 3- $h_2 =$ 1 μm.
Rys. 7. Tłumienność wtrącenia dla różnych grubości warstwy złota (ρ [g/cm^3], η [mPa·s): 1- $h_2 = 0{,}1$ μm; 2- $h_2 = 0{,}5$ μm; 3- $h_2 =$ 1 μm.

the gold layer thickness. When the thickness was increased only on one side of the quartz plate, the decrease of the amplitude took place on the same side, whereas it remained unchanged on the other side. For one of the SHAPMs, at a frequency of about 100.5 MHz, the amplitude of mechanical motion become twice as big when the gold layer thickness increased from about 0.1 μm to 1 μm. This effect was confirmed by measurements the SHAPM delay line insertion loss changes against viscosity of glycerine and water solutions for different gold layer thicknesses. Maximum sensitivity to viscosity changes is observed for thin gold layer. Lower sensitivity for thicker gold layers can be used for the changing ranges of viscosity measurements.

Acknowledgement

The authors would like to thank Marianna Baranowska for her assistance in making the drawings for this paper.

References

[1] Soluch W., Lysakowska M.: Properties of shear horizontal acoustic plate modes in BT-cut quartz, *IEEE Trans., Ultrason. Ferroelectr. Freq. Control*, 2011, 58, 2239 - 2243

[2] Nishikawa T., Tani A., Shirai K., Takeuchi C.: SH-type surface acoustic waves on Y-cuts quartz, *Proc. IEEE Frequency Control Symp*., 1980, 286 - 291

The influence of reducing agents on the reduced graphene oxide specific surface area determined on the basis of nitrogen adsorption isotherm

Tomasz Strachowski[1], Michał Woluntarski[1], Małgorzata Djas[1], Krystian Kowiorski[1], Zbigniew Wiliński[1], Magdalena Baran[1], Joanna Jagiełło[1], Magdalena Winkowska[1], Ludwika Lipińska[1]

The most common way to determine the specific surface of materials is to utilise direct methods, such as the flow method and the adsorptive method with the implementation of the adsorption isotherm equations. In our work we used the Brunauer, Emmet and Teller (BET) equation for the nitrogen adsorption isotherm description. Our goal was to examine the influence of reducing agents on the specific surface area of reduced graphene oxide. Graphene oxide was reduced by thiourea dioxide, thiourea, ammonium thiosulfate and sodium hydrosulfite.

Key words: graphene oxide (GO), reduced graphene oxide (rGO), specific surface area, adsorption, BET methods

Wpływ substancji redukujących na wielkość powierzchni właściwej zredukowanego tlenku grafenu określoną na podstawie izotermy adsorpcji azotu

Do określania powierzchni właściwej materiałów najczęściej stosowane są metody bezpośrednie, takie jak metoda przepływowa oraz adsorpcyjna, w której wykorzystywane są równania izotermy adsorpcji. W naszej pracy do określenia powierzchni właściwej zredukowanego tlenku grafenu do opisu wyznaczonej izotermy adsorpcji azotu zastosowano równanie Brunauera, Emmeta i Tellera (BET). Celem niniejszej pracy było zbadanie wpływu substancji redukujących na wielkość powierzchni właściwej zredukowanego tlenku grafenu. Do badań użyto tlenku grafenu redukowanego dwutlenkiem tiomocznika, tiomocznikiem, tiosiarczanem amonu, oraz podsiarczynem sodu.

Słowa kluczowe: tlenek grafenu (GO), zredukowany tlenek grafenu (rGO), powierzchnia właściwa, adsorpcja, metoda BET

1. Introduction

The specific surface area is the measure of an external surface area of a solid, recalculated per its mass unit and usually expressed in $m^2\ g^{-1}$. This parameter reflects physicochemical properties of materials that determine their applications, e.g. as catalysts in chemical reactions or photovoltaic cells.

Depending on the utilized physicochemical phenomena and measuring apparatus, the methods of the specific surface area determination can be divided into direct and indirect. Indirect methods are based on the knowledge of the grain-size distribution and material density. The specific surface area, defined as the external surface area per mass unit, is determined numerically through a distinction of various types of graining and summing the areas of individual grains. The main weakness of the indirect methods lies in their low accuracy, which depends on the number of the grain types distinguished and the grain shape.

Direct methods enable much more accurate measurements of specific surface area. These methods take into account the external surface area of the material examined, together with open pores, but excluding closed pores, which have no connection with the exterior. The following methods belong to this group:

- flow methods – the specific surface area measurement is based on the properties of a laminar Poiseuille-type flow through a laminar layer. In this method, a Blaine apparatus is most often used for measuring the specific surface area;
- porosimetric methods – consisting in the determination of the pore size in the material studied. The measurement is here based on the phenomena related to the behavior of wetting liquids in capillaries;
- adsorptive methods – apply the equation of monolayer adsorption (Langmuir) isotherm and the Brunauer, Emmet and Teller (BET) equation of multilayer adsorption isotherm.

On the basis of the literature review [8 - 17, 26 - 28], it can be stated that BET method gives the best possibility to obtain the most accurate values of the specific surface area that correspond to the real surface area. However, the BET measurements are time-consuming and require

[1] *Institute of Electronic Materials Technology*, 133 Wólczyńska Str., 01-919 Warsaw, Poland, e-mail: Tomasz.Strachowski@itme.edu.pl

sophisticated measuring apparatus. The BET method is a typical laboratory method, thus it is very accurate. As it happens we are in the posession of such equipment in the laboratory so this very technique for specific surface area examination was the most natural choice.

In our work we adopted the adsorptive method based on multilayer adsorption theory, elaborated by Brunauer, Emmett and Teller (BET). The fundamental assumption of this theory is the applicability of Langmuir equation to each adsorbed layer. It is assumed that the adsorbent becomes uniformly covered with a multilayer of molecules and the first adsorbed layer acts as a substrate for the successive layers, forming adsorptive complexes [1-7]. The number of adsorbed molecules depends on vapour pressure (p_0). The following equation of an adsorption isotherm was used in the measurements:

$$\frac{p}{V(p_0 - p)} = \frac{1}{V_m C} + \left(\frac{C - 1}{V_m C}\right) \times \frac{p}{p_0}, \qquad (1)$$

where: C is a constant, V - the total volume of the adsorbed gas, V_m – the volume of gas in the case of a complete coverage of the whole adsorbent surface with a monolayer and p/p_0 denotes the ratio of the measured pressure to the saturated vapour pressure of the adsorbate at the measurement temperature.

Basing on the above equation, we established various models of a measuring apparatus for the determination of the specific surface area [8 - 10], depending on the expected area value. The improvement of the measurement accuracy, requires high vacuum (10^{-5} Tr) and low temperature (at least as low as 100 K in case of nitrogen). Before the experiment, the samples are degassed and then the amount of adsorbed gas on the examined material surface is measured. Thus, we are able to determine the adsorption isotherms and also the volume of the gas adsorbed on a monolayer. The adsorbed gas volume can be easily recalculated into the number of adsorbed molecules.

If the surface occupied by one molecule is equal to α per the total surface area of the material examined, then:

$$S = \frac{V_m \times N_A}{V_{mol}}, \qquad (2)$$

$$\alpha = 1.09 \left(\frac{M}{N_A \rho}\right)^{2/3}, \qquad (3)$$

where N_A is Avogadro number (6.02×10^{23}), V_m – the molar volume of gas under the experimental conditions, V_{mol} – molar volume of adsorbate, M – the molecular weight and ρ denotes the density of the adsorbate.

The BET measurements can be performed using various gases: nitrogen, argon, helium, xenon, carbon dioxide [11 - 17]. In this work we used nitrogen. This gas is usually used in the BET surface analysis due to its availability in a high degree of purity and its strong interactions with most of the solids. Since the interaction between gas and solid phases is usually weak, the surface needs cooling by liquid nitrogen in order to obtain the detectable amounts of the adsorbate. Next, definite amounts of nitrogen are progressively released into the sample-containing chamber. The production of partial vacuum conditions allow lower relative pressure than atmospheric pressure. The value of α for nitrogen, given by Emmett and Brunauer, is 16.2×10^{-16} cm^2. For loose materials, BET method is regarded as the most adequate method for the determination of specific surface area as a physicochemical boundary between a solid and the surrounding gas or the liquid phase on a molecular level. This method is applied in the laboratories dealing with catalysis, surface structure of solids, powder metallurgy and ceramic powder technology for special applications, e.g. nuclear reactor cores. Thanks to the knowledge of the development of specific surface area it is possible to determine the usability of a given material for its further treatment and its prospective applications.

2. Experimental

The goal of the experiment was to examine the influence of synthesis conditions and reducing agents on specific surface area of reduced graphene oxide. In this paper we describe the measurements of the specific surface area of the starting material (graphite), graphene oxide and reduced graphene oxide.

2.1. Methodology

Specific surface area measurements were performed using a Quadrasorb Evo analyzer (Quantachrome Instruments). This apparatus consists of a FLOVAC Degasser degassing station and an analytic station, both of them shown in Fig. 1. The analyzer is equipped with a computer software which helped to control the experiment and

Fig. 1. An apparatus for the measurement of specific surface area (a) and a sample degassing station (b).
Rys. 1. Urządzenie do pomiaru powierzchni właściwej (a) oraz stacja do odgazowywania próbek (b).

record the data during the adsorption and desorption processes. This is a fully automatic system that allows to measure specific surface area in the range from 0.01 $m^2 g^{-1}$ to 6000 $m^2 g^{-1}$. [18].

Before the measurements the samples were degassed in vacuum for 5 hours. Graphene oxide was degassed at 323 K, because higher temperature could have caused its reduction inside the degassing station. Graphite and reduced graphene oxide were degassed at 523 K. For each sample analyzed, 13 measuring points were collected within the relative pressure range 0.05 - 0.30 p/p_0. Adsorption measurements were carried out using nitrogen at temperature 77 K.

Morphology analysis was performed with an AURIGA Cross Beam Workstation (Carl Zeiss) scanning electron microscope (SEM) [19].

2.2. Materials and synthesis

The investigations on the influence of the reduction conditions on specific surface area were carried out with the use of graphene oxide (GO) and reduced graphene oxide (rGO). Asbury 1 graphite was used as a starting material [20].

In the first stage, Asbury 1 graphite was oxidized to graphene oxide (GO) applying Marcano method [21 - 25] with the use of a mixture of nitric acid, ortophosphoric acid and potassium permanganate. The oxidation process was conducted in the temperature range 318 - 328 K within 5 hours. After the oxidation termination the product was purified in order to remove acids and other post-reaction impurities. The purified material was subjected to a chemical reduction by both organic and inorganic reducing agents. Graphene oxide used for the reduction was denoted as GO_A1 (after "Asbury 1").

The following reducing agents were chosen for the reduction of graphene oxide:

- **SAMPLE 1**
  Suspension with GO_A1 (2 mg ml^{-1}) + thiourea + metallic catalyst.
- **SAMPLE 2**
  Suspension with GO_A1 (2 mg ml^{-1}) + NaOH + sodium hydrosulfite.
- **SAMPLE 3**
  Suspension with GO_A1 (2 mg ml^{-1}) + ammonium thiosulfate.
- **SAMPLE 4**
  Suspension with GO_A1 (2 mg ml^{-1}) + thiourea dioxide.

Sample 1 was obtained by mixing 250 ml of GO with thiourea and a metal catalyst substrate. Ammonia was added to the resulting suspension to obtain pH = 11.80. The process was carried out in a glass reactor for 6 hours at 95°C. At the end of the process, the suspended material was repeatedly washed with deionized water and then dried to obtain a powder. Sample 2 was prepared by mixing 250 ml of GO with sodium hydrosulfite in the presence of NaOH. The process was carried out in a glass reactor for 6 hours at 95°C . At the end of the process, the suspended material was repeatedly washed with deionized water and then dried to obtain a powder. Sample 3 was prepared by mixing the GO suspension with ammonium thiosulfate. The process was carried out on a magnetic stirrer for 10 hours in a temperature range 95 - 100°C . Sample 4 was obtained by mixing the GO suspension with thiourea dioxide. The process was carried out in a glass reactor for 4 hours at 85° C. At the end of the process, the suspended material was repeatedly washed with deionized water and then dried to obtain the powder.

3. Results and discussion

The results of the specific surface area measurements for the reference samples, i.e. graphite and graphene oxides, and for the reduced graphene oxide samples are given in Tab. 1. Since the material examined was not homogeneous, 4 measurements were performed for each sample. An average value from these 4 measurements was taken

Tab. 1. Values of specific surface area according to reducing agents applied.
Tab. 1. Wartości powierzchni właściwej w zależności od zastosowanego reduktora.

Sample	Reducing agent	Specific surface area [$m^2 g^{-1}$]
Asbury 1 graphite	-	1
Graphene oxide	-	8
1	Thiourea	58
2	Sodium hydrosulfite	285
3	Ammonium thiosulfate	35
4	Thiourea dioxide	478

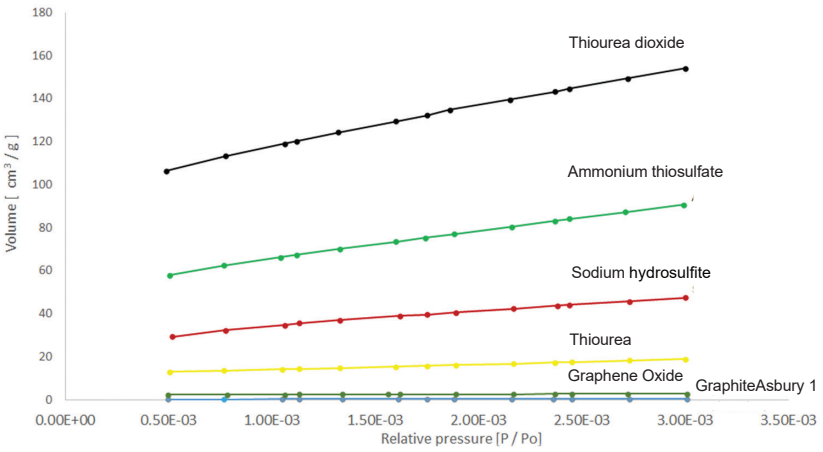

Fig. 2. Dependence of the adsorbed nitrogen volume per mass unit for various adsorbents on the pressure normalized with respect of the adsorbate saturated vapour pressure at the measurement temperature.
Rys. 2. Zależność objętości zaadsorbowanego azotu na jednostkę masy od ciśnienia znormalizowanego względem prężności pary nasycyonej adsorbatu w temperaturze pomiaru.

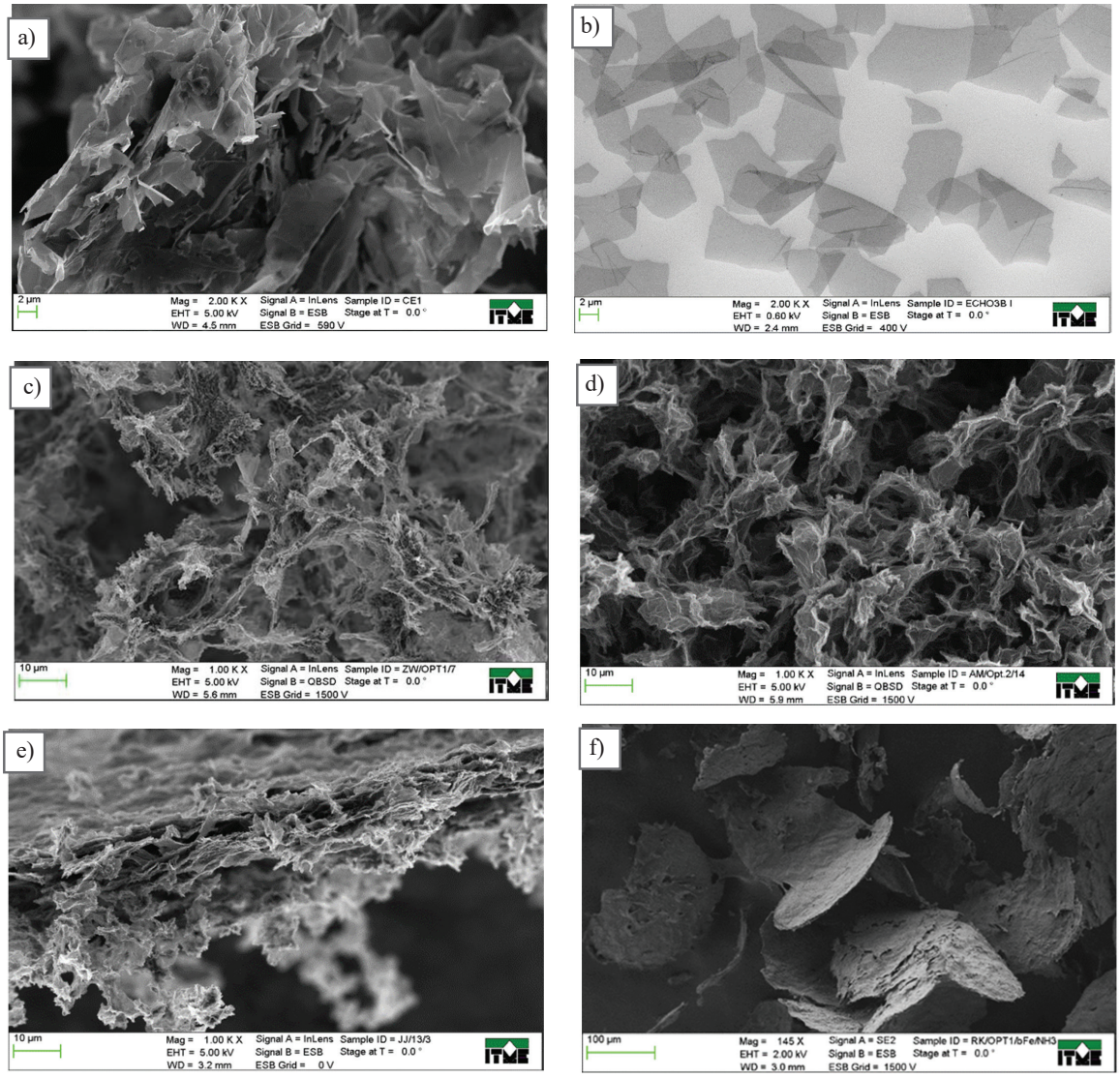

Fig. 3. Images of materials surface obtained by scanning electron microscopic (SEM): a) Asbury 1 graphite; b) graphene oxide; c) rGO obtained by GO reduction with thiourea; d) rGO obtained by GO reduction with sodium hyposulfite; e) rGO obtained by GO reduction with ammonium thiosulfate; f) rGO obtained by GO reduction with thiourea dioxide.
Rys. 3. Zdjęcia powierzchni otrzymane za pomocą mikroskopu skaningowego SEM: a) grafitu Asbury 1; b) tlenku grafenu; c) rGO otrzymany w wyniku redukcji tlenku grafenu tiomocznikiem; d) rGO otrzymany w wyniku redukcji tlenku grafenu podsiarczynem sodu; e) rGO otrzymany w wyniku redukcji tlenku grafenu tiosiarczanem amonu; f) rGO otrzymany w wyniku redukcji tlenku grafenu dwutlenkiem tiomocznika.

as the actual result. For each sample, the specific surface area values were determined in 13 measuring points of the BET isotherm in the range of relative pressure from 0.05 to 0.30 p/p_0. The experimental error is ± 3.97 $m^2 g^{-1}$.

Fig. 2 shows the dependence of adsorbed nitrogen volume ($cm^3 g^{-1}$) on the relative pressure (p/p_0). The measurements were conducted in the range of relative pressure from 0.05 to 0.30. This is a standard specific surface area measuring range.

On the basis of the specific surface area measurements by the BET method we can observe an important dependence of these values on the kind of a reducing agent applied and the reduction process conditions. Fig. 2 shows that the value of the specific surface area becomes greater with the increasing amount of adsorbed nitrogen. According to a correlation, the BET adsorption isotherms are usually linear for relative pressure within the range of 0.05 - 0.30 p/p_0. For the relative pressure lower than 0.05 the experimental points usually tend to deviate towards underrated values (greater V values) because the BET theory does not take into consideration the fact of energetic heterogeneity of the adsorbent surface. On the other hand, for the relative pressure higher than 0.35 the adsorption is often smaller than that predicted by Eq. (1), therefore the experimental points exhibit positive deviations.

The effect of the reducing agent application is also evident in scanning electron microscopic (SEM) images. Figs. 3a - f show the morphology changes from graphite, through graphene oxide, up to reduced graphene oxide.

4. Conclusions

The aim of the presented research was to examine the influence of reducing agents on the specific surface area of the reduction product, i.e. reduced graphene oxide. The inhomogeneity and morphology of the material obtained affect the value of the specific surface area, which can be visible in scanning electron microscopic (SEM) images. On the basis of SEM observations we can state that utilizing various reducing agents in the process of graphene oxide reduction enables us to obtain products of a diverse morphology. Graphene oxide is present in the form of flakes (see Fig. 3b), while after reduction these flakes become agglutinated, have uneven edges and are more porous.

The differences in the values of the specific surface area may also result from the presence of functional groups and elements which remained on the surface of the reduced graphene oxide. Those groups can hinder gas (i.e. nitrogen) adsorption on the surface of the examined material. Annealing and degassing the samples before the measurements does not allow these groups to be fully removed, and it referes especially to the groups covalently bound to the graphene flakes. Small amounts of sulfur embedded into the obtained reduction product result directly from the application of the reducing agent and, to a lesser degree, from the catalyst. The existence of the unremoved functional groups may cause the agglutination of graphene oxide flakes, and thus lead to the formation of agglomerates. Oxygen functional groups contained in the graphene material after the reduction process completion occurred in a moderate degree, which confirms the efficiency of the process conducted with the use of the aforementioned reagents. The best specific surface area was obtained for graphene oxide reduced by thiourea dioxide. The purity of the materials studied can be determined by FTIR analysis, which will be a subject of further research.

Acknowledgements

The authors are indebted to Mr. Andrzej Marcjaniuk for the performance of numerous reduction processes of graphene oxide and to Ms. Magdalena Romaniec for morphology analysis by scanning electron microscope.

References

[1] Brunauer S., Emmett P. H., Teller E.: Adsorption of Gases in Multimolecular Layers, *J. Am. Chem. Soc*., 1938, 60, 309

[2] Kordek J., Gawenda T., Kępys W.: Powierzchnia właściwa proszków, porównanie wyników policzonych i zmierzonych metodami przepływowymi i adsorpcyjnymi, *Górnictwo i Geoinżynieria*, 2006, 30, 3/1

[3] Dai J.-F., Wang G.-J., Ma L., Wu C.-K.: Surface properties of graphene: relationship to graphene-polymer composites, *Rev. Adv. Mater. Sci.,* 2015, 40, 60 – 71

[4] Sing K.: The use of nitrogen adsorption for the characterisation of porous materials, *Colloids and Surfaces A: Physicochemical and Engineering Aspects* 2001, 187 – 188, 3 – 9

[5] Gadipelli S., Guo Z. X.: Graphene-based materials: Synthesis and gas sorption, storage and separation, *Progress in Materials Science,* 2015, 69, 1 – 60

[6] Marban G.: BET adsorption reaction model based on the pseudo steady-state hypothesis for describing the kinetics of adsorption in liquid phase, *Journal of Colloid and Interface Science,* 2016, 467, 170 – 179

[7] Gomez-Serrano V., Gonzalez-Garcıa C. M., Gonzalez-Martın M. L.: Nitrogen adsorption isotherms on carbonaceous materials. Comparison of BET and Langmuir surface areas, *Powder Technology,* 2001, 116, 103 – 108

[8] Pajdak A., Skoczylas N.: Porównanie powierzchni właściwej i rozmiarów porów węgla metodami sorpcyjnymi w różnych temperaturach, *Prace Instytutu*

Mechaniki Górotworu PAN, 2014, 16, 3 – 4, 85 – 92

[9] Gauden P., Furmaniak S., Terzyk A.: Węgiel aktywny w ochronie środowiska i przemyśle, Pozorność a realność pola powierzchni materiałów węglowych otrzymywanych z modelu BET, Wyd. Politechniki Częstochowskiej, 2008, 95 – 103

[10] Choma J., Jaroniec M., Ustinov E.: Adsorpcyjna charakterystyka węgli aktywnych o bardzo dobrze rozwiniętej porowatości, *Ochrona Środowiska*, 2004, 4, 3 – 7

[11] Ramakrishna Matte H. S. S., Subrahmanyam K. S., Rao C. N. R.: Synthetic aspects and selected properties of graphene, *Nanomaterials and Nanotechnology*, 2011, 1, 3 – 13

[12] Srinivas G., Zhu Y., Piner R., Skipper N., Ellerby M., Ruoff R.: Synthesis of graphene-like nanosheets and their hydrogen adsorption capacity, *CARBON*, 2010, 48, 630 – 635

[13] R. Canty, E. Gonzalez, C. MacDonald, S. Osswald, H. Zea, C.Luhrs: Reduction expansion synthesis as strategy to control nitrogen doping level and surface area in graphene, *Materials*, 2015, 8, 7048 – 7058

[14] Si W., Wu X., Zhou J., Guo F., Zhuo S., Cui H., Xing W.: Reduced graphene oxide aerogel with high–rate supercapacitive performance in aqueous electrolytes, *Nanoscale Research Letters,* 2013, 8:247

[15] Birch E., Ruda – Eberenz T., Chai M., Andrews R., Hatfield R.: Properties that influence the specific surface areas of carbon nanotubes and nanofibers, *Ann. Occup. Hyg*., 2013, 57, 9, 1148 – 1166

[16] Guo F., Creighton M., Chen Y., Hurt R., Kulaots I.: Porous structures in stacked, crumpled and pillared graphene-based 3D materials, *CARBON,* 2014, 66, 476 –484

[17] Kaniyoor A., Baby T. T., Ramaprabhu S.: Graphene synthesis via hydrogen induced low temperature exfoliation of graphitic oxide, *Supplementary Material (ESI) for Journal of Materials Chemistry*, 2010

[18] http://www.quantachrome.com/index.html

[19] http://www.zeiss.com/

[20] http://www.asburystore.com/

[21] Marcano D. C., Kosynkin D. V., Berlin J. M., Sinitskii A., Sun Z., Slesarev A., Alemany L. B., Lu W., Tour J. M.: Improved Synthesis of Graphene Oxide, *ACS Nano*, 2010, 4 (8), 4806 – 4814

[22] Gómez I., Mejía E., Cabanzo R.: Synthesis of graphene oxide and chemically reduced graphene nanosheets, *Revista Colombiana de Materiales,* 2014*,* 5, 177 – 184

[23] Peng S., Fan X., Li S., Zhang J.: Green synthesis and characterization of graphite oxide by orthogonal experiment, *J. Chil. Chem. Soc.*, 2013, 58, 4

[24] Wojtoniszak M., Mijowska E.: Controlled oxidation of graphite to graphene oxide with novel oxidants in a bulk scale, *J. Nanopart Res.,* 2012, 14(11): 1248

[25] Sheshmanil S., Fashapoyeh M. A.: Suitable Chemical Methods for Preparation of Graphene Oxide, Graphene and Surface Functionalized Graphene Nanosheets, *Acta Chim. Slov*. 2013, 813, 60, 813 – 825

[26] Szymańska-Czaja M.: Porównanie metod pomiaru powierzchni właściwej materiałów drobno uziarnionych ze względu na zastosowanie tej wielkości w niektórych procesach technologicznych, *Gospodarka Surowcami Mineralnymi*, CPPGSMiE PAN, 1997, 13, 197 – 204

[27] Radomski P., Jarosiński A.: Wyznaczanie powierzchni właściwej materiałów ziarnistych w aspekcie stosowania jej wielkości w wybranych procesach technologicznych, *Chemia Czasopismo Techniczne*, 2010, 107, 267 – 276

[28] Allen T.: Particle Size Measurement London, Chapman and Hall LTD, 1971

Preparation of a BiTeI polar semiconductor with a strong asymmetric inversion

Andrzej Materna[1]

The paper describes the synthesis and crystallization processes of a BiTeI polar semiconductor, carried out by a modified vertical Bridgman method (VB), or/and by CVT (chemical vapor transport) method, in a horizontal position. For BiTeI samples, the measurements were performed by Van der Pauw method and by the structural techniques (EDS, XRD and Raman spectroscopy), which confirmed the presence of a pure BiTeI phase in the obtained materials.

Key words: topological insulator, BiTeX (X = I, Br, Cl) compounds, VB method, CVT method

Otrzymywanie polarnego półprzewodnika BiTeI, wykazującego silną asymetrię inwersji

W pracy opisano procesy syntezy i krystalizacji polarnego półprzewodnika BiTeI metodą transportu chemicznego (CVT) w układzie poziomym oraz zmodyfikowaną, pionową metodą Bridgmana (VB). Dla przygotowanej serii próbek, wykonano pomiary własności transportowych (metodą Van der Pauwa), które wykazały dużą ruchliwość nośników, w temperaturze 77K. Badania strukturalne wykonane za pomocą technik mikroanalizy rentgenowskiej EDS (energy dispersive spectroscopy), rentgenowskiej analizy dyfrakcyjnej XRD (X-ray diffraction analysis) oraz spektroskopii Ramana, potwierdziły obecność czystej fazy BiTeI w otrzymanych materiałach.

Słowa kluczowe: izolator topologiczny, związki BiTeX (X = I, Br, Cl), krystalizacja metodą VB, krystalizacja metodą CVT

1. Introduction

The subject area related to the existence of topological insulators dates back to 2008 [1]. In condensed matter physics, the appearance of a topologically protected state on the surface of a 3D topological insulator and the related phenomena originate from the presence of a strong Spin--Orbit Interaction (SOI) and Time Reversal Symmetry (TRS). This class of insulators is represented by symmetrical compounds, such as: Bi_2Se_3, Bi_2Te_3, Sb_2Te_3 [2]. The great value of spin-orbit coupling can lead not only to the formation of the phases of a topological insulator or to unconventional superconductivity [3 - 4], but also to other quantum effects.

One of the aforementioned phenomena referes to electron spin polarization in the absence of an applied external magnetic field, known as the *Rashba effect*. The Rashba effect splitting a momentum-dependent spin bands in 2D condensed matter systems (heterostructures and surface states), is similar to the splitting of particles and anti-particles in the Dirac Hamiltonian [1].

The Rashba effect results in the removal of degeneracy and splitting of the oppositely spin-polarized states of electrons (spin-split) [5]. This mechanism is schematically shown in Fig. 1 in a diagram of the band structure for the BiTeI material in its conduction band [3].

The possibility to observe such unique quantum effects within a single system makes the materials with a great value of spin-orbit coupling promising for their use in spintronics. The name Spintronics (spin electronics) is used to stress that it refers to the electron spin and not the electron charge. The key requirement is the ability to change the spin not in the magnetic but in the electric

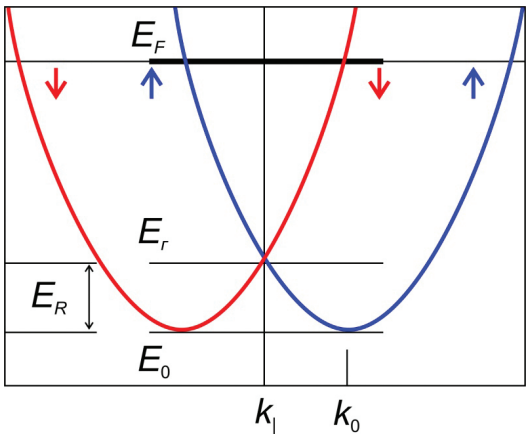

Fig. 1. Band structure diagram of BiTeI, with a visible spin splitting (displacement) *Rashba effect* - in the conduction band. E_F - Fermi level, E_R - Rashba energy, $E_0 = E_\Gamma$ - size of the energy gap. Colors indicate the opposite polarity of spins (spin-up, spin-down) [3].

Rys. 1. Schemat struktury pasmowej w BiTeI, z widocznym rozszczepieniem (przesunięciem) spinu *efekt Rashby*, w paśmie przewodnictwa. E_F - poziom energii Fermiego, E_R - energia Rashby, $E_0 = E_\Gamma$ - wielkość przerwy energetycznej. Kolorami oznaczono spiny o przeciwnej polaryzacji [3].

[1] *Institute of Electronic Materials Technology*, 133 Wólczyńska Str., 01-919 Warsaw, Poland, e-mail: Andrzej.Materna@itme.edu.pl

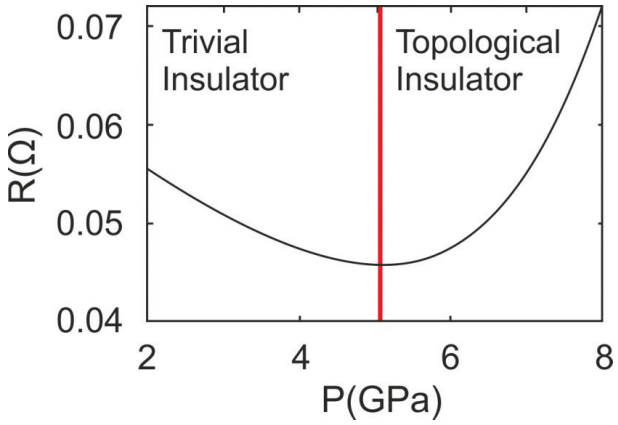

Fig. 2. Resistance - *R* (Ω) of BiTeI semiconductor, as a function of pressure *P* (GPa). At the level of ca. 5 GPa, the boundary (red line) of the phase transition from a trivial insulator state (polar semiconductor) to a topological insulator state becomes visible [11].

Rys. 2. Oporność - *R* (Ω) półprzewodnika BiTeI, w funkcji ciśnienia *P* (GPa). Na poziomie ok. 5 GPa, widoczna jest granica (czerwona linia), przejścia fazowego ze stanu izolatora trywialnego (polarnego półprzewodnika) do stanu izolatora topologicznego [11].

field. During the flow of a spin-polarized current, both the electric charges and the spins are being transferred, i.e. it is a flow of carriers (electrons or holes) with a specific spin. One of the goals of spintronics is to control the electron spin and as such it was applied in *spin-field* devices and in spin Hall effect transistors. [6 - 8]. The operation of spintronic devices utilizes the interaction between spin magnetic moment of the electron and the effective magnetic field. This interaction is of a relativistic nature and results from relativistic quantum mechanics, based on Dirac equations [9].

The crystalline compounds described above are represented by a BiTeI polar semiconductor, belonging to a new class of bismuth-tellurium ternary halides of the formula BiTeX (X = I, Br, Cl). These compounds are characterized by an asymmetric, inverted structure and by one of the greatest values of the Rashba coefficient, which amounts to αR ~3.8 eVÅ, while for other materials this coefficient is of the order of αR ~ (0.1 - 0.3) eVÅ, [5]. Therefore, BiTeI can be used as a primary material in fast switching systems, quantum computers and - in the near future- it may provide a basis for the development of a new field of physics, namely *semiconductor spintronics* [6]. Additionally, the phase transitions are possible in the BiTeI system, making it the only material, where the transition from a topologically trivial state (semiconducting state) to a topological insulator state and then to a topological superconducting state can be tested [4, 7].

Under atmospheric pressure conditions, BiTeI is a polar semiconductor (a trivial insulator), in which large Rashba splitting and energy gap can be observed. The calculated energy gap for the BiTeI system, based on the density functional theory (DFT), is $E_\Gamma \sim 0.8$ eV. When ignoring the spin-orbit interaction (SOI) [10], this value is almost twice as high as that obtained experimentally. Under the influence of the applied external pressure of the order of several GPa, this semiconductor undergoes the band inversion and a transition to a topological insulator state (Fig. 2) [11], making the BiTeI compound one of the first examples of the realization of a topological phase transition. Such a pressure-induced topology transformation in the structure of BiTeI is reversible [12]. Moreover, at higher pressures exceeding 10 GPa, the appearance of a topological superconducting state becomes possible [5].

The occurrence of the aforementioned transition is related to the quality of the crystal. As it is well known the low resistance of this material results from the presence of various defects [11]. Therefore, it becomes extremely important to find a method for the production of BiTeI crystals with a very high resistance. The first step to obtain such crystals is the synthesis of high purity components.

The synthesis of the BiTeI compound has proceeded according to the overall chemical equation:

$$Bi_2Te_3 + BiI_3 \rightarrow 3BiTeI,$$

where: Bi_2Te_3 - is a symmetrical topological insulator, BiI_3 - bismuth halide (iodide) - (Fig. 3).

A detailed description of the synthesis process is given in Section 2.1.

The structures of compounds: Bi_2Te_3 and BiTeI are schematically presented below. Fig. 3a shows a part of a layered structure of a hexagonal crystal lattice of a symmetrical topological insulator Bi_2Te_3, with a five-layer (quintuple) symmetrical unit cell. On the other hand,

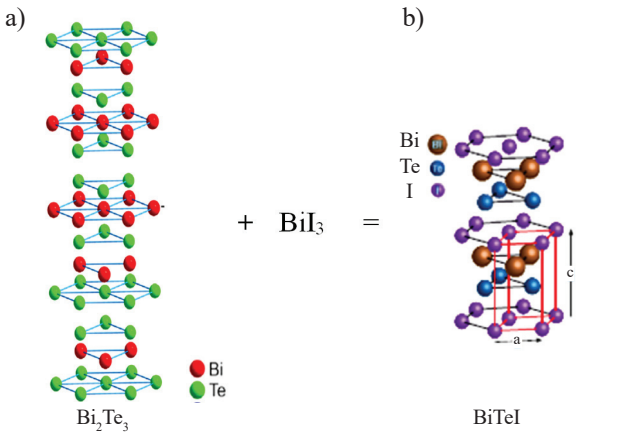

Fig. 3. The BiTeI compound structure, a) symmetrical unit cell (quintuple layers) of a Bi_2Te_3 topological insulator, b) asymmetrical unit cell with inversion of a BiTeI insulator with the dimensions indicated. Lattice parameters of BiTeI compound in the hexagonal plane a, along the growth axis – c are: a = 4.34 Å and c = 6.854 Å (according to Ishizaka *et al.*[5]).

Rys. 3. Struktura związku BiTeI, a) Symetryczna, pięciowarstwowa (kwintetowa) komórka izolatora topologicznego Bi_2Te_3, b) Asymetryczna z inwersją - komórka elementarna związku BiTeI, z widocznymi rozmiarami. Parametry sieci krystalicznej BiTeI w płaszczyźnie sześciokątnej - a, wzdłuż osi wzrostu - c, wynoszą: a = 4,34 Å i c = 6,854 Å (wg Ishizaka *et al.*[5]).

Fig. 3b shows the unit cell of a synthesized asymmetrical BiTeI semiconductor, which is also characterized by a hexagonal crystal lattice. In the three-layer (triple), asymmetrical unit cell of BiTeI, we can see the inversion of atomic layers arranged in the following order along the vertical direction of the c axis: I-Bi-Te-I-Bi-Te-I ...

The key component in the BiTeI lattice (in Fig. 3b) is bismuth (Bi), a heavy element whose atom exhibits a strong SOI. Its triangular layer is asymmetrically arranged between tellurium (Te) and halogen (I or Br, or Cl) layers. A layer of Bi, together with a layer of Te, i.e. an element of a similar lattice geometry to that of metallic bismuth, form a positively charged layer (BiTe)+. The zones of Van der Waals interactions occur between the layers of tellurium (Te) and iodine (I).

The concentration of *n-type* carriers in this material, obtained by Ishizaka *et al.* [5], was as high as $n_{bulk} \sim 4.5 \cdot 10^{19}$ cm^{-3}. According to Tournier-Colletta *et al.* [13], the lattice parameters for the BiTeI semiconductor are: a = 4.341 Å and c = 6.852 Å. However, the lattice, parameters of BiTeI, calculated by Shiyi Zhou *et al.* [10], are a = 4.32834 Å, c = 6.90572 Å. The authors assumed their data to be in agreement with the experimental results, i.e. a = 4.3392 Å, c = 6.854 Å, because of a small deviation from the measured values, i.e. not exceeding 1.5%.

2. Experimental - preparation and examination of BiTeI semiconductor

2.1. Synthesis of BiTeI compound

The phase diagram of the ternary compound Bi-Te-I (Fig. 4a) shows that the synthesis reaction can also result in other products formed under similar conditions, but of different chemical formulas, reflecting their different compositions, e.g.: C_1 - BiTeI, C_2- Bi_4TeI, C_3 - $Bi_4TeI_{1.25}$.

In order to determine the temperature for the synthesis process of the BiTeI compound, we used a pseudo-binary system BiI-Te (Fig. 4b). However, for the *laboratory* synthesis of the BiTeI insulator, we considered a phase diagram of the pseudo-binary, in which the components (reactants) for the synthesis were: BiI_3 and bismuth telluride - Bi_2Te_3.

The synthesis of the BiTeI compound proceeded in the etched and evacuated quartz ampoules, where the weighted samples of two compounds were placed: BiI_3 and a topological insulator - Bi_2Te_3 (according to Fig. 3).

Bismuth iodide - BiI_3 with a purity of ca. 99.5% is hygroscopic, quickly undergoes oxidation, and most of all, it is very toxic. For this reason, it was loaded in anaerobic chambers, in the atmosphere of a dry inert gas (f.e. Ar). The second reactant, i.e. bismuth telluride - Bi_2Te_3, as a raw material of high purity (at least 5N), was prepared earlier in a separate process, before the proper synthesis of BiTeI. Then, the loaded quartz reaction ampule of

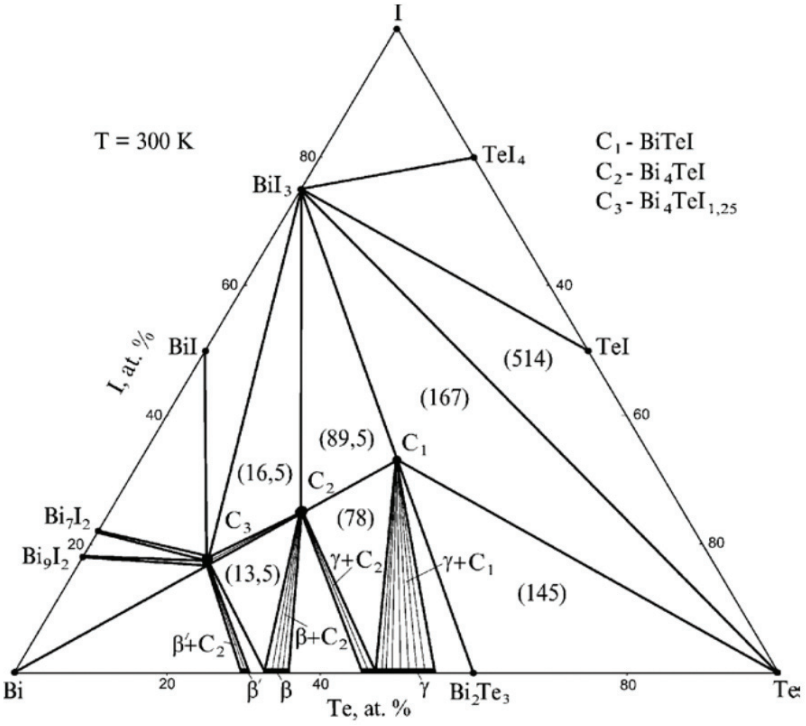

Fig. 4a. Phase diagram in the isothermal section (300 K) for Bi-Te-I [14].
Rys. 4a. Diagram fazowy w układzie izotermicznym dla: Bi-Te-I (300 K) [14].

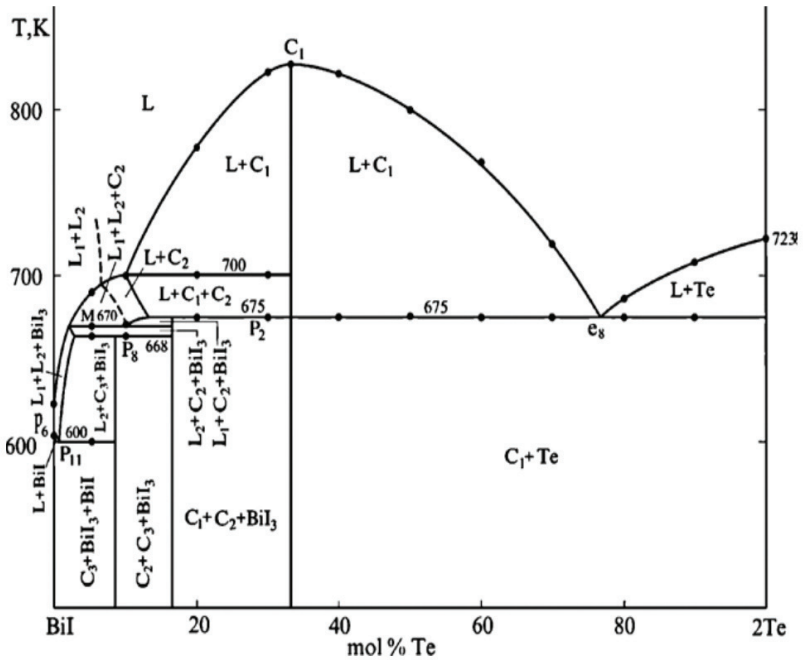

Fig. 4b. Phase diagram in the pseudobinary BiI-Te system [14].
Rys. 4b. Diagram fazowy w pseudo-binarnym układzie BiI-Te [14].

a diameter of 24 mm was placed in a three-zone resistance furnace. The homogeneous thermal field was characterized by an axial temperature gradient of ranging 2 - 3°C/cm and the maximum temperature did not exceed 640°C. The synthesis process took ~ 30 hours.

2.2. Crystallization of BiTeI

BiTeI semiconductor crystals can be obtained by several methods of crystallization, e.g. CVT, VB, HB, etc. This article focuses on CVT and VB methods.

1. The horizontal CVT (*Chemical Vapor Transport*) method in I_2 vapor is a two-step process. In the first stage, components BiI_3 and Bi_2Te_3 undergo a stoichiometric synthesis. After BiTeI crystallization, the ampoule content is unloaded. In the second stage, the quartz ampoules are loaded with a weighted samples of the prepared BiTeI precursor by placing it in the source zone of the ampoule, together with a weighted sample of iodine. The sublimating iodine serves for a transport agent of the particles from the source zone (at higher temperature) to the deposition zone (at lower temperature). When the vacuum reached the level of p ~ 4 x 10^{-6} Tr, the ampoule was sealed and placed in a horizontal furnace for the deposition of layers by the CVT method - see a diagram in Fig. 5. Due to a rapid evaporation of iodine vapors, iodine (I_2) loading took place under special conditions, with the use of a refrigerant.

2. The vertical VB (*Vertical Bridgman*) method is a one-step process. The synthesis and crystallization processes take place in one quartz ampoule, which is loaded with stoichiometric weighted samples of BiI_3, together with the previously prepared Bi_2Te_3. Then, after the vacuum reaches the level of p ~ 4 x 10^{-6} Tr, the ampoule was sealed and positioned in the upper zone of a vertical furnace for the crystallization of BiTeI.

The letter C denotes the material obtained by CVT method, e.g. BTI-C2.

During the first stage of the work, the measurements of temperature distribution in the horizontal furnace (Fig. 5) were carried out, in the temperature range 350 - 500°C, and in the vertical furnace, in the temperature range 250 - 600°C. The measurements of other technological parameters were also performed, namely:

a) axial temperature gradients in the source and deposition zones in the horizontal furnace; the time of BiTeI deposition process was selected on the basis of the precursor decomposition time - in the CVT method.

b) vertical and radial temperature gradients along the axis in the vertical furnace and the crystallization rate - v_k in the assumed thermal conditions - in the VB method.

In the second stage, the processes of the synthesis and deposition of the layers of BiTeI were carried out by the CVT method. The synthesis and crystallization of BiTeI were carried out by the VB method, according to the assumed parameters.

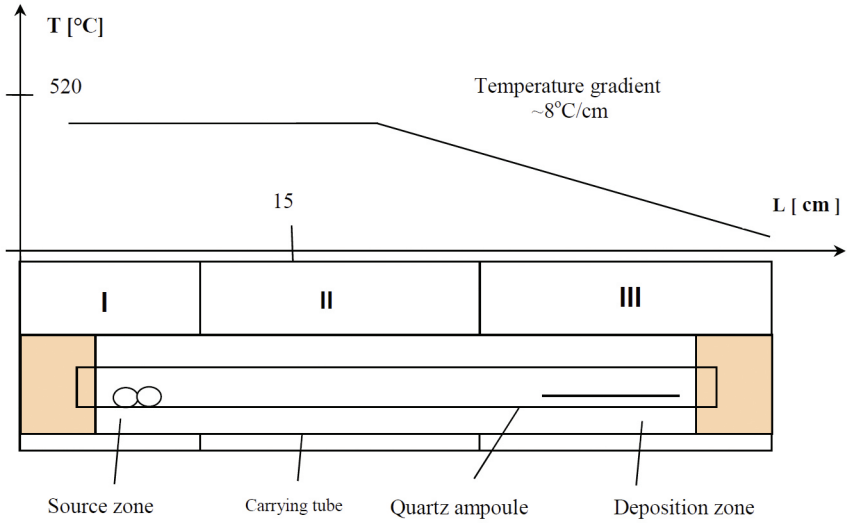

Fig. 5. Schematic temperature distribution in a three-zone (I, I, III) horizontal furnace in the temperature range 500 - 350°C, in the source and deposition zones, respectively, for the crystallization of BiTeI by CVT (Chemical Vapor Transport) method in I_2 vapor.
Rys. 5. Schematyczny rozkład temperatury w piecu poziomym, trójstrefowym (I, II, III), w zakresie temperatur: 500 - 350°C, odpowiednio w strefie źródłowej (z prekursorem) i w strefie osadzania, dla krystalizacji związku BiTeI metodą CVT, w parach I_2.

2.2.1 Crystallization of BiTeI compound by CVT method

After a preliminary synthesis of the BiTeI precursor, loading the reactants and the evacuation of the air from the reaction ampoule, the ampoule was placed in a horizontal furnace (Fig. 5) and the process of BTI-C1 deposition was performed by the CVT method. The total deposition time took ca. 150 hours.

As a result of the BTI-C1 process, a small monocrystaline plate (Fig. 6) of the following dimensions: 6 × 8 × 0.1 mm^3, precipitated on the inner wall of the ampoule, in the middle of its length.

After the composition determination by the XRD method, it was found that the lines of the visible peaks did not overlap with those indicated for the standard of a BiTeI material. The obtained phase was Bi_2Te_3, which became separated from the BiTeI precursor and crystallized as a single crystal wafer in a horizontal system. The measurement carried out in the plane of the wafer, showed hkl (001 lines), characteristic of Bi_2Te_3, indicating (001) orientation on the wafer - Fig. 7.

The possible cause of this phenomenon was the evaporation of some part of the mass of iodine - I_2, assumed as the particle transporting agent, while obtaining the vacuum in the reaction ampoule and the decomposition of the BiTeI precursor.

In the next BiTeI crystallization process, the mass of iodine was increased, the pumping time was shortened by a half, the final vacuum level was reduced to 2 x 10^{-5} Tr, the deposition time was increased and the mass of the BiTeI precursor was left at the same level. Then the growth of the BTI C2 was carried out.

As a result of the BTI C2 process, two parts of the deposited BiTeI insulator layers were obtained in the initial and terminal parts of the reaction ampoule - (Fig. 8a).

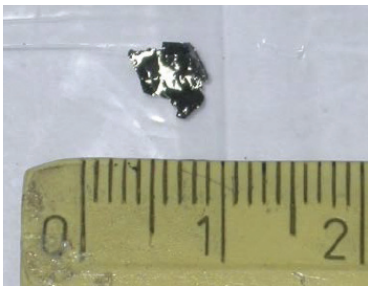

Fig. 6. A layer deposited in the BTI C1 process, as a single crystal wafer - Bi_2Te_3.
Rys. 6. Osadzona warstwa, w procesie BTI C1, w postaci monokrystalicznej płytki Bi_2Te_3,

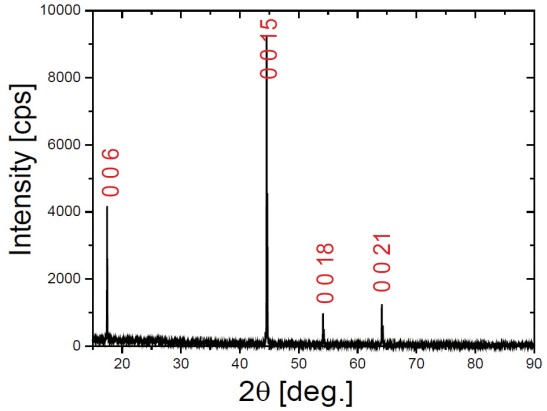

Fig. 7. Diffraction pattern (XRD) of a sample from BTI C1 process; visible single crystal cleavage plane of (001) crystallographic orientation. The indicated indexes of the observed reflections correspond to a Bi_2Te_3 phase (SG R-3m).
Rys. 7. Dyfraktogram XRD próbki z procesu BTI-C1; widoczna monokrystaliczna płaszczyzna łupliwości o orientacji (001). Oznaczone indeksy obserwowanych refleksów dyfrakcyjnych, odpowiadają fazie Bi_2Te_3 - (SG R-3m).

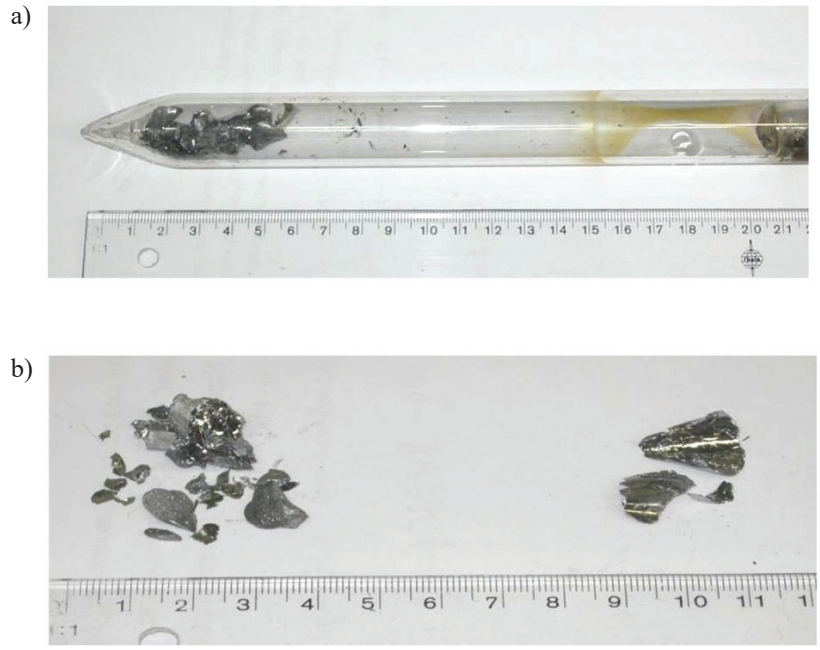

Fig. 8. Preparation of BiTeI semiconductor in BTI C2 process by CVT method in a horizontal configuration: a) view of the reaction ampoule, b) the reactants of the precursor (left side) and the deposited BiTeI layers (right side).
Rys. 8. Proces BTI C2 metodą CVT w układzie poziomym, półprzewodnika BiTeI; a) widok ampuły reakcyjnej), b) substraty prekursora (po lewej) i osadzone warstwy BiTeI (po prawej stronie).

Fig. 8a shows the horizontal view of the ampoule after the BTI-C2 semiconductor growth by the CVT method. In its initial, conical part we can see the disintegrated pieces of the BiTeI precursor and the layer deposited on the walls of the ampoule in the source temperature zone. In its opposite part (right end), we can observe the second portion of the deposited layer (in the deposition zone) and a yellowish precipitate after the crystallization of iodine vapor. Fig. 8b shows the view after unloading the reaction ampoule and the separation of the pieces of the synthesized precursor, i.e. the BiTeI compound (left side) from the deposited BiTeI layers (right side). The visible conical shape of the latter sample results from the internal shape of the conical part of the ampoule, on which the layer was deposited. The entire size of the deposited layer was around 25 × 15 mm^2 and its thickness was around 0.2 - 0.4 mm^2. The total time of the layer deposition process took around 350 hours. The crystal lattice parameters in the hexagonal plane -a and along the growth axis -c, were determined during the XRD phase analysis of this layer and are discussed below.

Fig. 9 presents the result of the phase composition analysis, performed by the XRD method for the layers obtained from a BTI-C2 process. We can see the reflections characteristic of a BiTeI material.

Fig. 10 shows the result of a Raman spectroscopic examination of the composition of the layers obtained from a BTI-C2 process. These data are similar to those reported by M. K. Tran et al. [9].

After the examination of the phase composition using both methods, it was found that the obtained layers formed

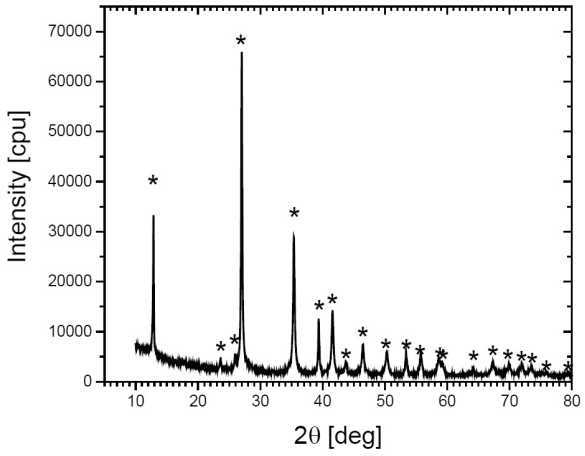

Fig. 9. Diffraction pattern (XRD) of a powdered layer obtained in BTI-C2process. The diffraction reflections corresponding to a pure BiTeI phase are indicateed by the symbol * (SG P3).
Rys. 9. Dyfraktogram sproszkowanej warstwy z procesu BTI-C2. Symbolem * oznaczono refleksy dyfrakcyjne odpowiadające czystej fazie BiTeI (SG P3).

a pure phase of the BiTeI semiconductor, without any precipitates of foreign phases.

2.2.2 Crystallization of BiTeI compound by VB method

As mentioned before, the vertical crystallization of the BiTeI semiconductor was performed using the VB method. The reaction ampoule with a diameter d = 22 mm,

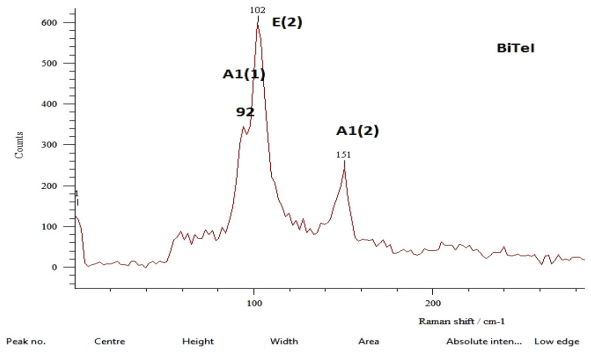

Fig. 10. Raman spectrum for a BTI-C2 sample, with the characteristic energies of modes of A1(1), A1(2) and E(2) symmetry for a pure BiTeI phase.
Rys. 10. Widmo Ramanowskie próbki BTI-C2 z charakterystycznymi dla czystej fazy BiTeI, energiami modów o symetriach A1(1), A1(2) i E(2).

previously loaded with the weighed reactants (BiI_3 and Bi_2Te_3) was exhausted (~ 4 x 10^{-6} Tr), sealed and placed in a vertical furnace. The maximum temperature of the melt was ca. 590°C, the axial temperature gradient was at the level of G_o ~ 26 °C/cm and the crystallization rate was: v_k ~ 4 mm/h. The total time of the crystallization process, together with the preparation was ca. 40 hours.

The BTI-1 crystal obtained in the crystallization process was characterized by the mass of ~ 35 g, diameter 18 mm and length 21 mm. Next, after cutting it perpendicularly to the growth axis (Fig. 11b), four wafers of the size 5 x 5 mm were sampled and subjected to exfoliation with a pressure-sensitive adhesive tape in order to remove a damaged layer. Then the samples went through the structural analyses by a scanning microscope (SEM and EDS) - Figs. 12 - 14.

In order to verify the quality of the obtained material, 12 points were chosen on the surface of the BTI-1/5 sample

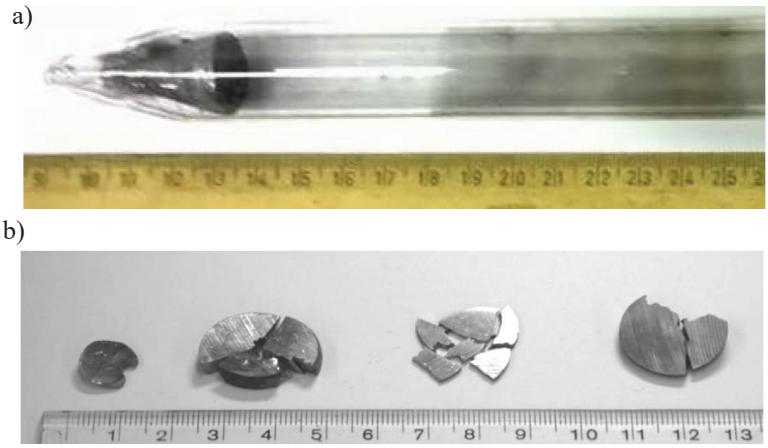

Fig. 11. a) View of the reaction ampoule after BTI-1 crystallization process; b) View of a BTI-1 crystal, after cutting it into the samples of various thickness (approx. 5 mm, 3 mm and 2 mm). The samples were destined for the structural, spectral and electrical measurements. Skew grains are visible on the wafers.
Rys. 11. a) Widok ampuły reakcyjnej z wsadem, po procesie krystalizacji BTI-1; b) Widok kryształu BTI-1 po przecięciu na różne grubości próbek (ok. 5 mm, 3 mm i 2 mm). Próbki przeznaczono na pomiary strukturalne, spektralne i elektryczne. Widoczne skośne ziarna na płytkach.

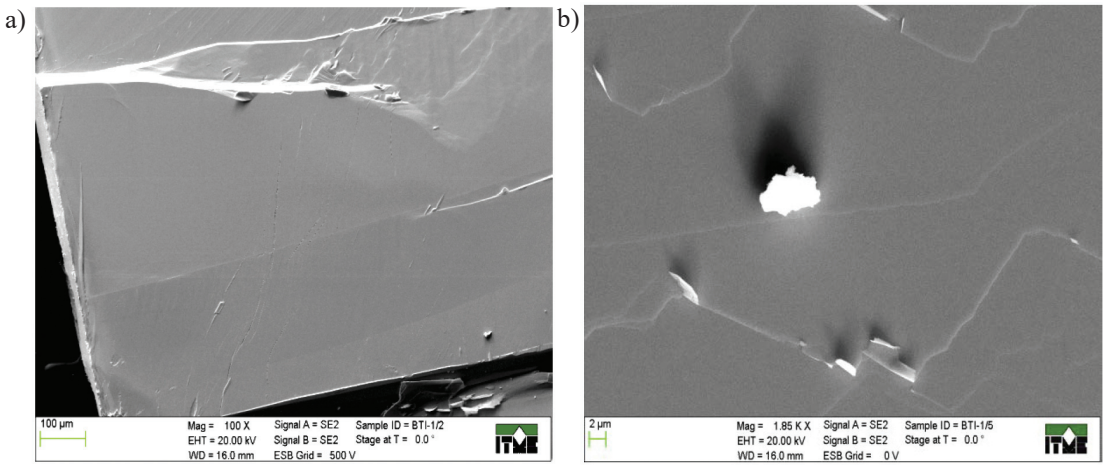

Fig. 12. SEM images of the wafers after exfoliation; visible large, homogeneous surfaces of BTI-1 wafers: a) BTI-1/2 with dimensions of approx. 900 x 600 µm^2, scale bar 100 µm. b) BTI-1/5 with the visible small parts (size 2 - 5 µm) from the previous exfoliation, scale bar 2 µm.
Rys. 12. Obrazy SEM płytek po eksfoliacji, widoczna duże jednorodne, powierzchnie płytek (ziaren) BTI-1. a) BTI-1/2 o wymiarach ok. 900 x 600 µm^2, znacznik 100 µm. b) BTI-1/5 widoczne małe naderwane fragmenty (kawałki) o wymiarach 2 - 5 µm z poprzedniej eksfoliacji. Znacznik 2 µm.

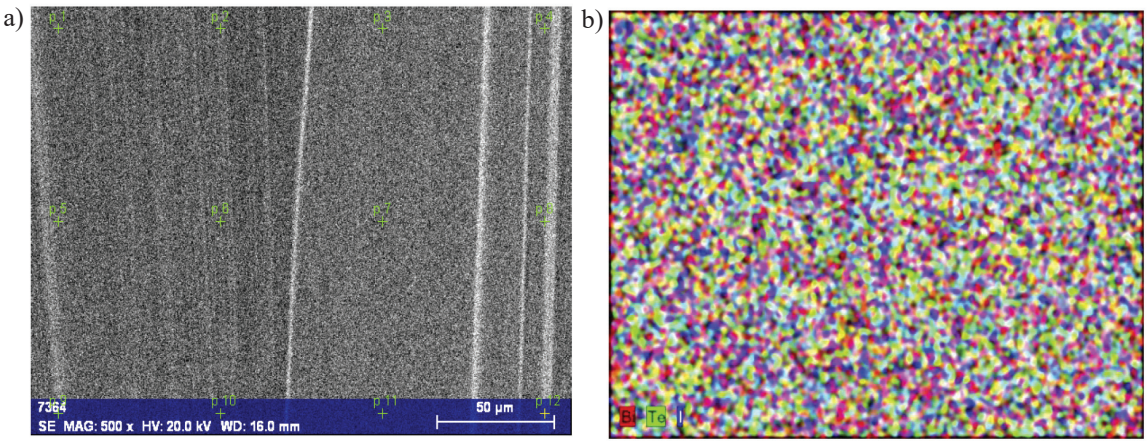

Fig. 13. a) SEM image of a BTI-1/5 wafer (dimensions of approx. 250 x 150 µm), with 12 measuring p 1 - p 12 points (green) for Tab. 1. b) EDS measurement showing a homogeneous, uniform distribution of the elements: Bi-red, Te- green and I -blue.
Rys. 13. a) Obraz SEM płytki BTI-1/5 o wymiarach ok. 250 x 150 µm. z 12 punktami pomiarowymi p 1 - p 12 (zielonymi), do Tab. 1. b) Pomiar EDS. Widoczny równomierny, jednorodny rozkład pierwiastków. Oznaczenia kolorów: Bi-czerwony, Te-zielony, I -niebieski.

Spectrum: p 3

El	AN	Series	unn. C [wt.%]	norm. C [wt.%]	Atom. C [at.%]	Error (1 Sigma) [wt.%]
C	6	K-series	0.00	0.00	0.00	0.00
Al	13	K-series	0.00	0.00	0.00	0.00
Te	52	L-series	26.68	28.81	34.56	0.79
I	53	L-series	25.98	28.05	33.84	0.76
Bi	83	L-series	39.96	43.14	31.60	1.28
		Total:	92.62	100.00	100.00	

Fig. 14. Local elemental analysis of a BTI-1/5 sample by EDS – data for spectrum p 3, Tab. 1.
Rys. 14. Analiza pierwiastkowa EDS dla próbki BTI-1/5, w punkcie – spectrum p 3, Tab. 1.

Tab. 1. Measurement of atomic composition of the elements: Te, I, Bi and the mean value (Te-34.79%, I -33.95%, Bi-31.26%) from 12 points (p 1 - p 12, green crosses - Fig. 13a), located on the wafer surface. The measurement error (sigma), ranges from 0.33 to 0.6%. The theoretical (ideal) distribution is 33.33% for each analyzed element.
Tab. 1. Pomiar składu atomowego pierwiastków: Te, I, Bi oraz uśredniony wynik (Mean value Te 34,79%, I 33,95%, Bi-31,26%) z dwunastu punktów p 1 - p 12 (zielone krzyżyki - Rys. 13a), położonych na powierzchni tej płytki. Błąd pomiarowy (Sigma) waha się od 0,33 do 0,6 %. Teoretyczny (idealny) rozkład wynosi 33,33(3)% dla każdego analizowanego pierwiastka.

Measuring point	Atomic percent (%)		
Spectrum	**Te**	**I**	**Bi**
p1	35.44	34.20	30.36
p2	35.08	34.46	30.47
p3	34.56	33.83	31.60
p4	34.96	33.74	31.30
p5	34.75	33.79	31.46
p6	34.86	33.94	31.20
p7	35.28	34.15	30.56
p8	34.63	34.02	31.35
p9	34.42	33.49	32.09
p10	34.39	34.36	31.25
p11	34.22	33.37	32.40
p12	34.62	34.09	31.29
Mean value:	34.79	33.95	31.26
Sigma:	0.36	0.33	0.60
Sigma mean:	0.11	0.10	0.17

for the measurements of the atomic composition homogeneity. The elements: Te, I and Bi were analyzed at the selected places - Fig. 13a. The results of the composition measurements are presented in Tab. 1.

Figures 15 and 16 show the results of the phase composition tests performed by Raman spectroscopy and XRD methods for the wafers of a size 5 × 5 mm^2, obtained in the BTI-1 process, after the exfoliation.

The XRD measurements were made in a Bragg-Brentano geometry (θ/2θ) - Figs. 7, 9 and 16, using a Rigaku SmartLab 3 kW diffractometer. The *Kα* radiation line of a Cu lamp was used, with the operating parameters: U = 40 kV and I = 30 mA. A Dtex linear detector was applied. The phase analysis and Rietveld analysis of the lattice parameter refinement was carried out using the PDXL program, associated with the ICDD PDF4+2015 crystallographic database.

The samples obtained in VB (BTI 1/2) and CVT (BTI C2) processes consist of a single BiTeI phase of a P3 trigonal structure (the standard number: ICDD 00-043-0650) and are characterized by the following lattice parameters (in the hexagonal notation):

BiTeI standard from ITME crystallographic database
a = 4.3394 Å c = 6.8626 Å

Layers obtained by CVT (BTI C2)
a = 4.3411 Å c = 6.8617 Å

Crystal obtained by VB (BTI 1/2)
a = 4.3412 Å c = 6.8587 Å

The lattice parameters of the layers and crystals obtained in ITME are: a = 4.3411 Å, c = 6.8617 Å and a = 4.3412 Å, c = 6.8587 Å, respectively. These values are consistent with the data reported by the authors from other research laboratories in the world [5,10,13].

In order to improve structural quality and increase the grain size, the next growth process of a BTI-2 semiconductor was carried out using the VB method, reducing the charge mass, the crystallization rate to v_k = 2.5 mm/h, and simultaneously increasing the axial temperature gradient to the level of G_o ~ 35°C/cm.

A BTI-2 crystal that was obtained as a result of the aforementioned process, had the mass of ~ 18 g, diameter 12 mm and length 16 mm, and the grain size ranging from 2 to 7 mm. Then, after cutting it perpendicularly to the axis of the growth (Fig. 17), the wafers with the dimensions of 5 × 5 mm^2 were taken for the electrical tests.

As shown in Fig. 17, the wafers obtained in the BTI-2 process have larger grains than those obtained in the BTI-1 process.

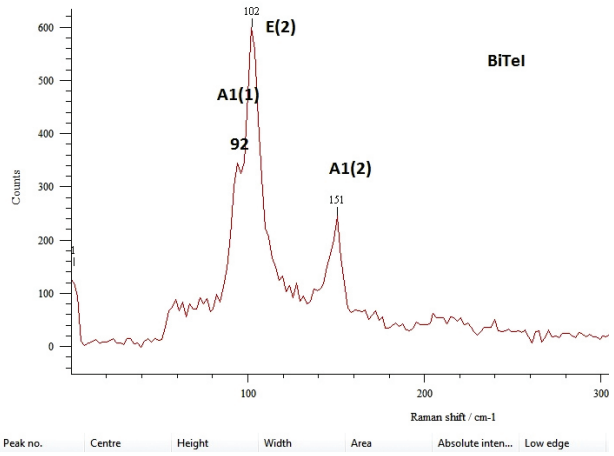

Fig. 15. Raman spectrum of a sample BTI- 1/4, with characteristic energies of modes for the phase of BiTeI (a pure phase without precipitates is visible).
Rys. 15. Widmo Ramanowskie próbki BTI- 1/4 z charakterystycznymi energiami modów dla fazy BiTeI, (widoczna czysta faza, bez wytrąceń).

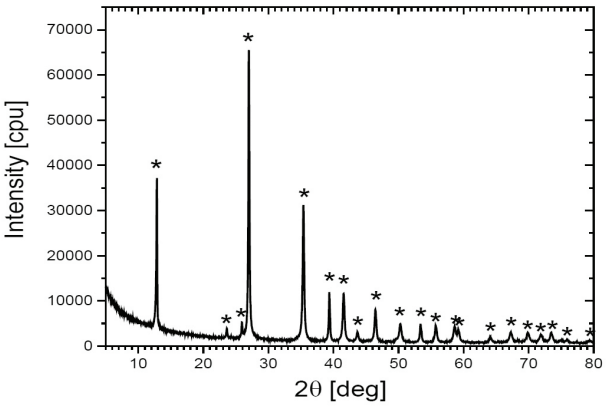

Fig. 16. Diffraction pattern (XRD) of a powdered layer of a BTI-1/2 crystal. A single phase of a BiTeI insulator is visible. Symbol * indicates diffraction reflections corresponding to the BiTeI phase (SG P3).
Rys. 16. Dyfraktogram XRD sproszkowanego kryształu BTI-1/2 widoczna pojedyncza faza izolatora BiTeI. Symbolem* oznaczono refleksy dyfrakcyjne odpowiadające fazie BiTeI (SG P3)

Fig. 17. BTI-2 crystal after cutting it into wafers of a thickness of approx. 4 mm, destined for the structural and electrical measurements.
Rys. 17. Kryształ BTI-2, po przecięciu na płytki o grubości ok. 4 mm. przeznaczone na pomiary strukturalne i elektryczne.

3. Measurements of electrical parameters of a polar semiconductor - BiTeI

Wafers measuring 5 x 5 mm^2 and the thikness $g = 0.4$ mm were prepared for the tests of the electrical properties of a BiTeI semiconductor by the Van der Pauw method. The results for the wafers originating from both crystallization methods (VB and CVT) are presented in Tab. 2. As an example, a photo of the samples obtained from the BTI-2 process and with the contacts soldered, is shown in Fig. 18. The measurements were carried out at temperature 295 K (RT) and 77 K.

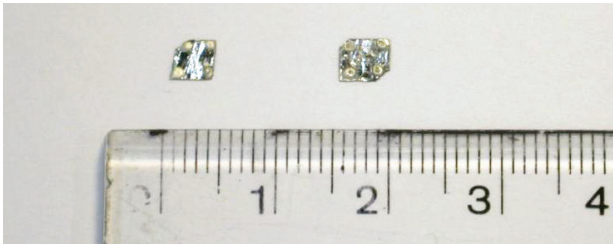

Fig. 18. The samples with the dimensions 5 × 5 mm, after exfoliation from the crystals: BTI-2/1 (left) and BTI-2/2 (right), with the soldered contacts (Ag), destined for electrical measurements by the Van der Pauw method.
Rys. 18. Eksfoliowane próbki o wymiarach 5 × 5 mm. z kryształu BTI-2/1 (lewa) i BTI-2/2 (prawa), z przylutowanymi kontaktami (Ag), przeznaczone do pomiarów elektrycznych metodą Van der Pauwa.

In accordance with the results obtained in transport measurements by the Van der Pauw method at room temperature (RT), presented in Tab. 2, in a layer originating from the BTI-C2 process and prepared by CVT, the carriers concentration of n-type was ca. twice lower than their concentration in the samples of the crystals obtained by the Bridgman vertical method (VB).The carriers mobility in the same sample (BTI-C2), was ca. twice as low in comparison with the mobility in a material obtained by the VB method. It could indicate a better structural quality and a greater purity of the samples of BiTeI crystals originating from VB processes.

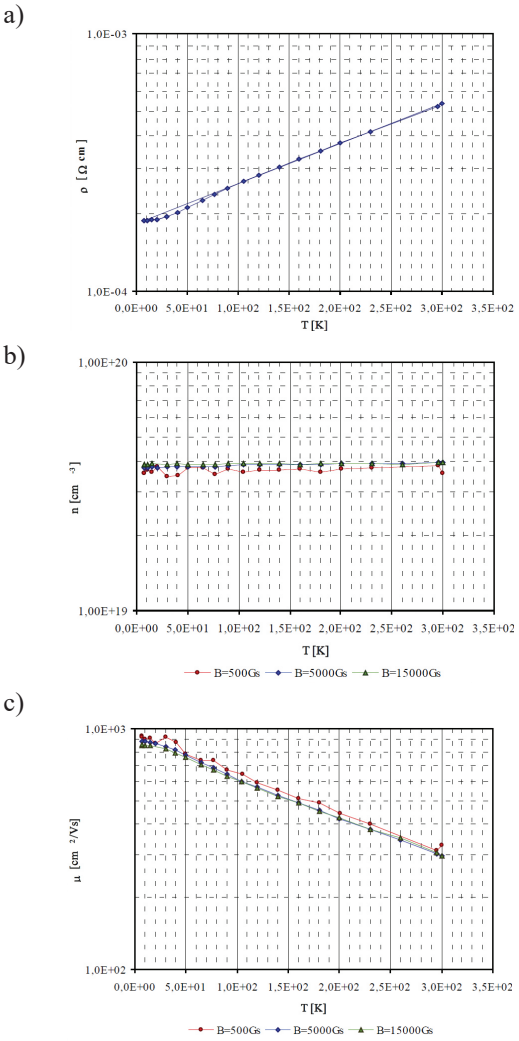

Fig. 19. Results of measurements of the electrical parameters for samples from the BTI-2/2 wafer: a) the resistivity $\rho = f(T)$, b) the carrier concentration $n = f(T)$, c) the mobility $\mu = f(T)$, as a function of temperature. N-type conduction exhibits a stable value over the whole measured temperature range.
Rys. 19. Wyniki pomiarów parametrów elektrycznych próbek z płytki BTI-2/2 w funkcji temperatury: a) oporności właściwej $\rho = f(T)$, b) koncentracji nośników $n = f(T)$, c) ruchliwości $\mu = f(T)$. Typ przewodnictwa n, wykazuje stabilną wartość w całym zakresie mierzonych temperatur.

Tab. 2. Measurements of the electrical parameters: carrier concentration n, mobility μ and resistivity ρ, for BiTeI semiconductor samples, obtained using the VB and CVT methods. Measurement temperature was 295 K (RT) or 77 K. All the samples examined were characterized by n-type conduction.
Tab. 2. Pomiary parametrów elektrycznych: koncentracji nośników n, ruchliwości μ i oporności właściwej ρ, dla próbek półprzewodnika BiTeI otrzymanych metodami VB i CVT. Temperatura pomiaru wynosiła 295 K (RT) lub 77 K. Wszystkie pomierzone próbki, posiadały przewodnictwo w typie n.

Methods	Sample number	Test temperature	n [cm^{-3}]	μ [cm^2/Vs]	ρ [Ωcm]	Conduction type
VB	BTI-1/3	295K-RT	4.70e19	2.80e2	5.53e-4	n
	BTI-1/3	77K	4.96e19	5.95e2	2.11e-4	n
	BTI-2/2	RT	3.93e19	3.04e2	5.22e-4	n
	BTI-2/2	77K	3.89E19	6.75e2	2.38e-4	n
CVT	BTI-C2/1	RT	2.65e19	1.67e2	1.41e-3	n
	BTI-C2/2	RT	2.34e19	1.96e2	1.36e-3	n

BTI-2/2 sample, was subjected to transport measurements to examine the influence of temperature (T in the range 15 - 295 K) on the following parameters: specific resistance ρ = f (T), carrier concentration n = f (T) and carrier mobility μ = f (T). The results are shown in Fig 19.

For a comparison, in Fig. 20 we show the results reported by M. Kanou and T. Sasagawa [3], concerning the in-plane resistivity vs. temperature dependence determined for the BiTeI crystals growing in the Bridgman vertical method (VB) and in the modified horizontal Bridgman HB method (Horizontal Bridgman). The BiTeI semiconductors obtained by the VB method were characterized by a concentration of n-type carriers at the level of $n \sim 6 \cdot 10^{19}$ cm^{-3}, while those obtained from the vapor phase by the VT method (Vapor Transportation) exhibited a single crystal structure and low electrical conductivity (electrical resistance greater than 1.5 MΩ at room temperature).

The above measurements show that the material obtained in ITME has the same type of conduction, i.e. n-type, and a similar resistivity at temperature 77 K ($\rho \sim 2 \cdot 10^{-4}$ Ωcm), as the material obtained by Sasagawa *et al.* and that it has a smaller carrier concentration ($n \sim 4 \cdot 10^{19}$ cm^{-3}) than that reported by the cited authors [3] ($n \sim 6 \cdot 10^{19}$ cm^{-3}).

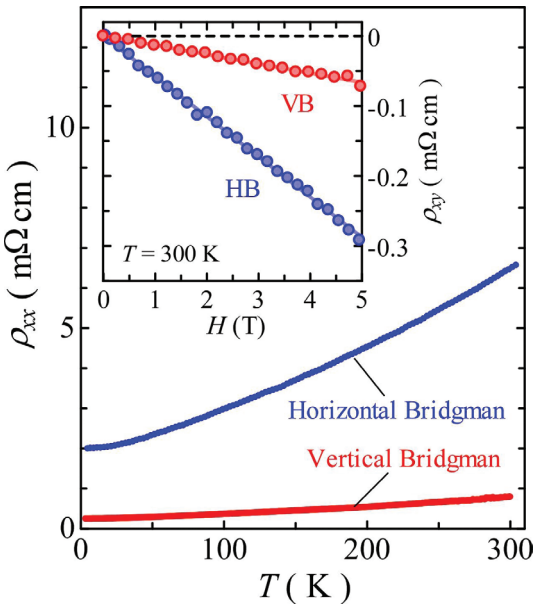

Fig. 20. Temperature dependence of in-plane resistivity (in ρ_{xx} plane) of BiTeI crystals grown by the standard vertical Bridgman (VB) method and the modified horizontal Bridgman (HB) method. Upper inset shows the dependence of Hall resistivity ρ_{xy} on magnetic field (measurements at room temperature – RT). [3]
Rys. 20. Zależność oporności właściwej (w płaszczyźnie ρ_{xx}) od temperatury, dla kryształów BiTeI wzrastających pionową metodą Bridgmana (VB) i zmodyfikowaną, poziomą metodą Bridgmana (HB). W górnej wstawce (inset), pokazano zależność oporności właściwej Halla ρ_{xy} od pola magnetycznego (H), (pomiary w temperaturze pokojowej - RT). [3]

4. Conclusions

Crystal layers of a polar semiconductor (trivial insulator) BiTeI, were obtained either by a stoichiometric synthesis and crystallization from pure elements, i.e. Te and Bi with bismuth halide BiI_3 in a quartz ampoule by the modified Bridgman method (VB) in a vertical system, or by the CVT method (chemical transport in iodine vapor) in quartz ampoules, where the previously synthesized BiTeI precursor was placed in the source zone. Iodine vapor acted as a transporting agent for the particles in a horizontal system. The wafers of dimensions 5 × 5 mm^2 were cut from the BiTeI semiconductor crystals obtained by both methods and the composition (using Raman and XRD spectroscopy), electrical properties (Van der Pauwa method) and structure (EDS) of these samples were investigated. The results confirmed the presence of a pure BiTeI phase, without precipitates, and with a uniform distribution of the constituent elements - Tab. 1.

When comparing both methods of the crystallization of the BiTeI compound, it becomes evidence that the higher the material yields the better was structural quality, obtained during a vertical crystallization using the VB method. The concentration of the majority carriers that we obtained for a BiTeI n-type semiconductor, ranging from $n \sim 2.3 \cdot 10^{19}$ to $4.9 \cdot 10^{19}$ cm^{-3}, and the resistivity at the level of $\rho \sim (5 - 17) \cdot 10^{-4}$ Ωcm, are similar to those obtained in other research centers [3, 5].

According to the reference database, the lattice parameters of BiTeI are: a = 4.3394 Å in the hexagonal plane and c = 6.8626 Å along the growth axis. XRD measurements of the layers and crystals obtained in ITME using the CVT and VB methods indicate the following values of lattice parameters: a = 4.3411 Å, c = 6.8617 Å and a = 4.3412 Å, c = 6.8587 Å, respectively. They are consistent with the data reported by other researches from various laboratories in the world, e.g to Tournier-Colletta et al. [13], where the lattice parameters for the BiTeI semiconductor amounted to: a = 4.3410 Å and c = 6.8520 Å. This data can be considered as reliable, since the deviation from the reference value is smaller than 0.5%.

A high quality BiTeCl topological insulator and a BiTeI polar semiconductor with a high theoretical value of Rashba coefficient, obtained in ITME, can be utilized for further analyses and work progress in the field of crystal growth technology of BiTeI crystals characterized by high resistance. Moreover, these materials may also open up the possibilities of a search for new quantum phenomena, such as unconventional superconductivity, spin transport and a new type of a topological non-conducting state, all arising from a unique electronic structure of these compounds. The results should also contribute to the development of a new field of physics, i.e. semiconductor spintronics.

Acknowledgements

The author would like to express their great thanks to Dr. Eng. Paweł Ciepielewski for the Raman spectroscopic measurements, to M.Sc. Magdalena Romaniec for EDS measurements, to Dr. Eng. Ryszard Diduszko for XRD analyses of the phase composition, to M.Sc. Mirosław Piersa for the measurements of electrical parameters and for M.Sc. Aleksandra Królicka for her help.

References

[1] Hsieh D., Qian D., Wray L., Xia Y., Hor Y. S., Cava R. J., Hasan M. Z.: A topological Dirac insulator in a quantum spin Hall phase, Nature, 2008, 452, 970 – 974

[2] Zhang H., Liu C. - X., Qi X. - L., Dai X., Fang Z., Zhang S. - C.: Topological insulators in Bi_2Se_3, Bi_2Te_3 and Sb_2Te_3 with a single Dirac cone on the surface, *Nat. Phys.,* 2009, 5, 438 - 442

[3] Kanou M., Sasagawa T.: Crystal growth and electronic properties of a 3D Rashba material, BiTeI, with adjusted carrier concentrations, *Journal of Physics Condensed Matter,* 2013, 25(13):135801

[4] Qi Y., Shi W., Naumov P. G., et. al., Topological quantum phase transition and superconductivity induced by pressure in the bismuth tellurohalide BiTeI, *Advanced Materials*, 2017, 29, 18, 1605965

[5] Ishizaka K., Bahramy M. S., Shin S., et al.: Giant Rashba-type spin splitting in bulk BiTeI, *Nature Materials*, 2011, 10, 7, 521 – 526

[6] Bercioux D., Lucignanoy P.: Quantum transport in Rashba spin-orbit materials: a review, *Rep. Prog. Phys*., 2015, 78, 10, 106001

[7] Sakano M., Bahramy M. S., Ishizaka K., et al.: Three--dimensional bulk band dispersion in polar BiTeI with giant Rashba-type spin splitting, *Phys. Rev. B,* 2012, 86, 085204

[8] Maaß, H., Bentmann H., Seibel Ch., et al.: Spin-texture inversion in the giant Rashba semiconductor BiTeI, *Nat. Commun.,* 2016, 7, 11621

[9] Tran M. K., Levallois J., Lerch P., et al.: Infrared- and Raman-Spectroscopy Measurements of a Transition in the Crystal Structure and a Closing of the Energy Gap of BiTeI under Pressure, *Phys. Rev. Lett.*, 2014, 112, 047402

[10] Zhou S., Long J., Huang W.: Theoretical prediction of the fundamental properties of ternary bismuth telluro-halides, *Materials Science in Semiconductor Processing*, 2014, 27, 605 – 610

[11] Van Gennep D., Linscheid A., Stewart G. R., et al.: Pressure-induced superconductivity in the giant Rashba system BiTeI, *J. Phys: Condens. Matter.*, 2017, 29

[12] Bahramy M. S., Yang B.-J., Arita R.: Emergence of non-centrosymmetric topological insulating phase in BiTeI under pressure, *Nature communications*, 2012, 3, 679

[13] Tournier-Colletta C., Autes G., Kierren B., et al.: Atomic and Electronic Structure of a Rashba p-n Junction at the BiTeI Surface, *Phys. Rev. B*, 2014, 89, 085402

[14] Babanly M. B., Tedenac J. C., Aliyev Z. S., et al.: Phase equilibriums and thermodynamic properties of the system Bi–Te–I, *J. of Alloys and Compounds*, 2009, 481, 1 – 2

LIST OF REVIEWERS 2017

dr Małgorzata Aleksandrzak
prof. dr hab. inż. Jerzy Filipiak
dr hab. inż. Dariusz Golański
dr hab. inż. Jacek Gołębiowski
dr Michał Hermanowicz
dr hab. inż. Paweł Kamiński
dr Mateusz Kempiński
dr inż. Konrad Kiełbasiński
prof. dr hab. Zbigniew Klusek
prof. dr hab. inż. Piotr Król
prof. dr hab. inż. Mikołaj Szafran
dr hab. inż. Michał Szymański
prof. dr hab. inż. Andrzej Świątkowski
dr hab. inż. Tomasz Wejrzanowski
prof. dr hab. inż. Marian Zaborski

INFORMATION FOR AUTHORS AND READERS

I. Submission rules

1. Only the manuscripts not published previously can be accepted. The author of the paper or the person submitting the manuscript of a multi-author work on behalf of all co-authors are required to declare that the work has not been published previously. If the test results contained in the manuscript have been presented earlier at a scientific conference or a symposium, the information on this fact should be given at the end of article containing the name, place and date of the conference. At the end of the article the authors should also provide the information on the sources of a financial support of the work, the contribution of scientific and research institutions, associations and other entities.

2. The manuscripts both in Polish and in English can be submitted. Due to introducing all the articles printed in *Electronic Materials* to the Internet , the author should make a statement on the copyright transfer of the author's economic rights to the Publisher.

3. Concerned about the reliability of the scientific work and the development of an ethical attitude of a researcher, a procedure has been introduced in order to prevent any cases of scientific dishonesty and unethical attitudes, defined as *ghostwriting* and *guest authorship* (*honorary authorship*):

- *ghostwriting* occurs when someone has made a substantial contribution to the publication without revealing his participation as one of the authors or without mentioning his role in the acknowledgments in the publication;
- *guest authorship* occurs when although the contribution of a given person is negligible or it has not taken place at all, he or she is an author/co-author of the publication.

The Editors require that the authors disclose the contributions of the individual authors in the preparation of a multi-author work, giving their affiliations and the information on their participation in the creative process, i.e. the information on the authors of the work's idea, assumptions, methods, etc. that have been utilized during the article preparation. The main responsibility for this information is borne by the author submitting the manuscript.

4. The Editors are obliged to keep the documentation of any forms of the scientific dishonesty, especially the violation of the ethical rules that are obligatory in science. All discovered cases of *ghostwriting* and "guest authorship" will be disclosed by the Editors, including the notification of the relevant entities, such as the institutions employing the authors, scientific societies, associations of scientific editors, etc.

II. Procedure of articles review and approval for print

1. The author's materials directed for print in "Electronic Materials" are subjected to evaluation by the independent reviewers and the members of the Editorial Board.

2. The reviewers are suggested by the thematic editors – the members of the Editorial Board, responsible for a given subject field.

3. At least two independent reviewers from outside the research institution affiliated by the author of the publication are called for the evaluation of each publication.

4. In case of a publication in a foreign language, at least one reviewer is called, affiliated in a foreign institution with the seat in a country other than that of the origin of the author of the manuscript.

5. The author or authors of the manuscript and the reviewers do not know their identities (the so-called "double-blind review process").

6. A review is in written form and contains a clear conclusion of the reviewer concerning the article acceptance for the publication (without corrections or with necessary amendments to be made by the author) or its rejection.

7. The criteria for the article acceptance or rejection and a possible review form are disclosed to the public on the website of *Electronic Materials.*

8. The names of the reviewers of the individual publications or the editions are not disclosed. Once a year, in the last issue of "Electronic Materials", a list of the cooperating reviewers will be made public.

9. The Editors of *Electronic Materials* may edit the material obtained, shorten or supplement it (after an agreement with the author), or not qualify it for the publication.

10. The Editor-in-chief refuses to publish the authors' materials in the following cases:

- the contents of the manuscript are illicit,
- any signs of the scientific dishonesty, and especially *ghostwriting* and *guest authorship*, will be found out,
- the work has not received a positive final evaluation from the reviewers and the thematic editor.

11. The Editor-in-chief may refuse to publish the article if:

- the topic of the work is not in line with the subject field of *Electronic Materials*,
- the manuscript exceeds the acceptable volume and the author does not agree to shorten the article,
- the author refuses to make any necessary amendments proposed by the reviewer and the Editorial Board,
- the text or the illustrations provided by the author do not meet the technical requirements.